Engineering Structures 275 (2023) 115232

Contents lists available at ScienceDirect

Engineering Structures

journal homepage: www.elsevier.com/locate/engstruct

Analytical model for the in-plane resistance of masonry walls retrofitted with steel fiber reinforced mortar coating

Luca Facconi *, Sara S. Lucchini, Fausto Minelli, Giovanni A. Plizzari

DICATAM - Department of Civil, Environmental, Architectural Engineering and Mathematics, University of Brescia, Italy

ARTICLE INFO

Keywords:
Masonry
Steel Fiber Reinforced Mortar
Coating
Retrofitting
In-plane resistance
Analytical model
Finite element analysis

ABSTRACT

Recent experimental tests showed the ability of Steel Fiber Reinforced Mortar (SFRM) coating to significantly improve the in-plane resistance of masonry walls and buildings. International and national structural codes, such as the fib Model Code 2010 (MC2010) and the Italian building code (NTC2018), have introduced fiber reinforced cementitious composites as structural materials for designing structural elements. However, the use of these materials as jacketing of masonry buildings is currently not taken into considerations by any design guidelines as potential seismic retrofitting intervention. Besides the limited availability of experimental data, this gap in design recommendations is closely related to the lack of design equations able to provide the shear and flexural resistance of retrofitted masonry elements.

The present work aims at filling this gap by proposing code-oriented formulations for calculating the in-plane lateral resistance of walls strengthened by SFRM overlays. The model has been mainly validated by comparison with the numerical results obtained from a comprehensive parametric study presented and described in the paper. Finally, an example is presented to show a practical application of the model.

List of Symbols

A_{sn}	area of the n^{th} vertical rebar placed in the tensile zone;
A'_{sn}	area of the n^{th} vertical rebar placed in the compressed zone;
b	factor depending on the stress distribution over the wall section;
d_n	effective depth of tensile vertical rebars;
d'_n	effective depth of compressed vertical rebars;
E	elastic modulus;
f_c	cylindrical compressive strength of SFRM;
f_{ck}	characteristic cylindrical compressive strength of SFRM;
f_{cm}	mean value of cylindrical compressive strength of SFRM;
f_{ct}	tensile strength of SFRM;
$f_{Ft-0.25}$	residual tensile strength at a crack width of 0.25 mm;
f_{Ft}	residual tensile strength of SFRM;
f_{Ft1}	residual tensile strength corresponding to w_1;
f_{Ftu}	residual tensile strength significant for ultimate conditions, corresponding to w_u;
f_m	compressive strength of URM;
$f_{mt,num}$	uniaxial tensile strength of URM;
$f_{mt} = 1.5\tau_0$	diagonal tensile strength of URM;
f_R	residual flexural tensile strength of SFRM;
f_t	tensile stress;
f_{v0}	shear (frictional) strength of unit-mortar interface at zero compression;
f_y	yield strength of vertical rebars;
G_c	compressive fracture energy;
G_f^I	mode-I fracture energy;
h	height of the wall;
$h_{ch} = A^{1/2}$	characteristic length;
k	factor accounting for the increase of masonry compressive strength after retrofitting;
L	total length of the wall;
m	redundancy factor for diagonal shear mechanism;
M_R	resisting moment;
$n = 1, 2$	number of SFRM coating layers;
N	wall axial force;
t_{coat}	thickness of the single SFRM coating layer;
t_m	thickness of the masonry panel;
v_{cr}	shear stress corresponding to first cracking;

* Corresponding author.
E-mail addresses: luca.facconi@unibs.it (L. Facconi), sara.lucchini@unibs.it (S.S. Lucchini), fausto.minelli@unibs.it (F. Minelli), giovanni.plizzari@unibs.it (G.A. Plizzari).

https://doi.org/10.1016/j.engstruct.2022.115232
Received 19 April 2022; Received in revised form 26 September 2022; Accepted 30 October 2022
Available online 24 November 2022

$v_{s,coat}$ frictional stress provided by SFRM coating;
$v_{s,m}$ frictional stress provided by URM;
V_d shear resisting force by dowel action of reinforcing bars;
V_R total lateral resistance;
V_R^{an} analytical value of total base shear;
V_R^{exp} experimental value of total base shear;
V_R^{num} numerical value of total base shear;
$V_{R,flex}$ lateral load causing flexural failure;
$V_{R,max}$ shear force causing diagonal crushing of masonry;
$V_{R,s}$ shear resistance related to sliding shear mechanism;
$V_{R,t}$ shear resistance related to diagonal shear mechanism;
$V_{t,coat}$ diagonal shear resistance of SFRM;
$V_{t,m}$ diagonal shear resistance of URM;
w crack width;
w_1 crack width corresponding to f_{Ft1};
w_u crack width corresponding to f_{Ftu};
x_f depth of the neutral axis for flexure;
x_s depth of the neutral axis for sliding shear;
$z = 0.8L$ approximate value of the internal lever arm;
$\alpha = 0.85$ coefficient taking into account the long-term effects on the compressive strength;
βh lever arm of lateral load;
δ lateral deflection of the wall;
$\varepsilon_c = 3.5$ ‰ ultimate compressive strain of masonry and SFRM coating;
ε_{sn} strain acting in the tensile vertical rebars;
ε'_{sn} strain acting in the compressed vertical rebars;
η strength reduction factor;
θ average slope of the struts;
$\lambda = 0.8$ factor defining the effective height of the compressed zone;
ν Poisson's coefficient;
σ_{coat} maximum bending stress acting in SFRM when sliding failure takes place;
σ_m maximum bending stress acting in URM when sliding failure takes place;
$\sigma_{s,max}$ maximum tensile stress acting in each rebar when splitting failure occurs;
σ_{sn} stress acting in the n^{th} tensile vertical rebar;
σ'_{sn} stress acting in the n^{th} compressed vertical rebar;
$\sigma_0 = N/(L \cdot t_m) > 0$ compressive stress acting normally to the wall cross-section;
$\sigma_{0,s} = N/(x_s \cdot t_m) > 0$ compressive stress acting normally to compressed zone 'x_s';
τ_0 shear strength (from diagonal compression test) of URM at zero compression.

1. Introduction

Retrofitting or repairing existing masonry building represents one of the main challenges of structural engineering that has involved several research studies worldwide. The most recent seismic events occurred in 2016 between four regions of central Italy highlighted, once again, the high vulnerability of these structures due to both out-of-plane and in-plane actions.

In order to improve the in-plane resistance of Un-Reinforced Masonry (URM) members, several techniques have been proposed during the last 20 years. Grout injections [1], external steel reinforcement [2], Fiber Reinforced Polymers (FRP) [3–6] and the application of concrete/mortar coating are just some of the potential and most widespread methods, whose advantages and disadvantages are well documented in the literature. Particular attention has been recently devoted to the development of techniques based on the use of reinforced coatings such as those adopting Engineered Cementitious Composites (ECC) [7,8], Fiber Reinforced Cementitious Mortar (FRCM – also known as Textile Reinforced Mortar) [9–12] and Steel Fiber Reinforced Mortar (SFRM).

In order to retrofit URM buildings with SFRM, a relatively thin layer (e.g., 20–60 mm thick) of mortar must be laid on either one or both sides of the walls to enhance the masonry strength by exploiting the high tensile strength of coating. The latter is due to the good post-cracking tensile performance of SFRM resulting from the use of discrete steel fibers randomly spread within the mortar matrix. This technique is effective if proper masonry-to-coating connectors [13] are installed and, moreover, the bond behavior of SFRM is good enough to prevent the separation of coating from the masonry substrate. A further resisting contribution can be provided by localized conventional reinforcement connecting SFRM coating to the wall foundation. To this purpose, vertical steel rebars placed within the coating thickness can be used to increase the bending as well as the sliding shear resistance of the wall, especially where the SFRM coating presents discontinuities (e.g. the wall-to-foundation interface). The potentialities and the drawbacks related to the use of this strengthening method are discussed by different research works [14–16], including some studies recently published by the Authors of this paper [17,18].

Since the studies focusing on masonry retrofitted with SFRM coating are still limited, the complete understanding of the mechanisms affecting the flexural and shear resisting mechanisms of retrofitted walls is still far to be fully achieved. In this context, the development of analytical models for predicting the behavior of strengthened members is quite complex. In fact, the lack of a comprehensive experimental database and harmonized test methods makes the model formulation and calibration difficult to perform. To compensate for the deficiency of experimental information, one may exploit the significant availability of finite element codes suitable for simulating masonry structures. Attempts to simulate masonry strengthened with SFRM coating have been successfully made by different Authors [17,19,20], who adopted finite element models based on well consolidated methods such as the smeared crack approach or the continuum damage mechanics.

If, on the one hand, the research on the adoption of SFRM coating for retrofitting masonry have experienced a progressive development, on the other, the application of the technique to real existing buildings is still far from an extensive and widespread use. Some structural codes, like the Italian standard NTC2018 [21] and the fib Model Code 2010 (MC2010) [22], have introduced, in the recent past years, design recommendations concerning steel fiber reinforced cementitious materials for structural use. However, both research and standards have not yet proposed theoretical models able to reasonably establish the in-plane capacity of masonry walls strengthened with SFRM coating. The present study aims at filling this gap by proposing a simple and practically oriented analytical model able to predict the lateral resistance of masonry walls retrofitted by SFRM overlays.

When considering walls retrofitted with reinforced mortar coating and subjected to in-plane lateral actions, either shear or bending failure mechanisms, like those traditionally considered for unreinforced masonry, may generally occur. In more detail, international standards and guidelines like NTC2018 [21], Eurocode 6 [23] and FEMA [24] identify the following three main mechanisms (Fig. 1):

- Diagonal shear failure, consisting of a main diagonal crack running across the central region of the masonry panel and coating layer.
- Shear sliding failure, characterized by an almost horizontal crack localized in the coating layer as well as along the interface between masonry joints and units.
- Flexural failure, which involves the flexural failure of coating together with a localized crushing of the wall compressed corner.

The analytical model described in the following sections idealizes masonry and coating as different bi-dimensional layers and bases its formulation on the following assumptions: (1) SFRM coating and masonry are perfectly bonded together. (2) Forces are transferred from masonry to coating through shear only. (3) Both masonry and coating resist only to in-plane actions. (4) The effect of geometrical asymmetry that characterizes the single-sided strengthened members is neglected. (5) Compatibility conditions are not taken into account when

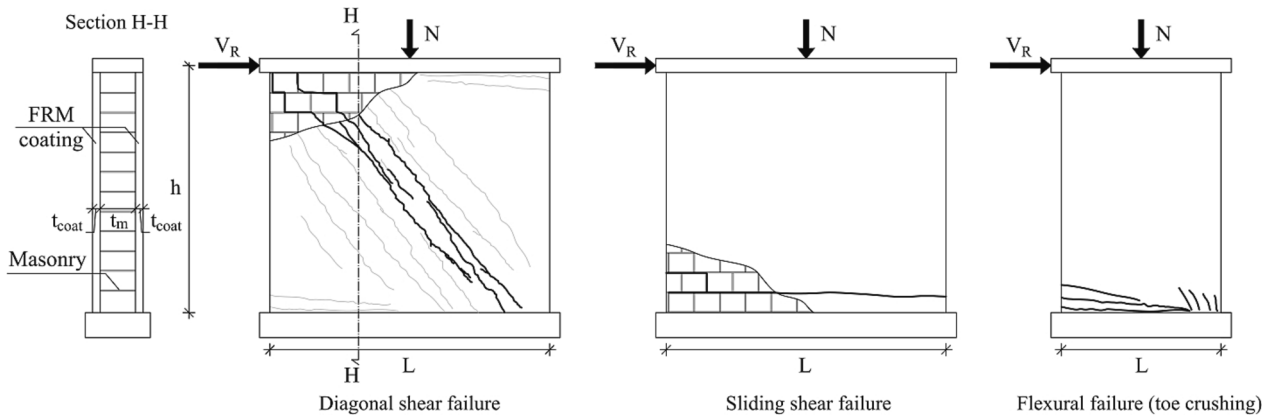

Fig. 1. Typical failure modes of strengthened masonry.

determining the strength of both the URM panel and the SFRM coating. (6) Considering the usual small thickness (i.e., ≤50 mm) of coating, the influence of coating self-weight on shear resistance can be neglected.

Regarding assumption (1), in order to ensure good bond conditions between coating and masonry, a surface preparation is recommended especially when the masonry surface is particularly smooth. In that case, it is recommended to prepare the wall surface by mechanical methods able to clean it and improve the surface roughness.

The proposed calculation procedure is straightforward as it is based only on the equilibrium and on material properties derived from codes or standardized material tests. As discussed above, few experimental data concerning tests on structural elements strengthened with SFRM coating are currently reported by literature. Because of this limited availability of experimental data, the validation of the analytical model was mainly based on the comparison with the results of a comprehensive parametric study involving several finite element simulations of cantilever and double fixed-end walls having different geometrical and material properties. The parametric study was carried out with a well consolidated smeared crack finite element model, whose reliability was proven by simulating both the full-scale walls and the full-scale building described in Section 3.1.

It is worth remarking that the analytical model has been formulated to predict only the in-plane resistance of masonry walls. A future paper will be devoted by the Authors to present an analytical model specifically developed to predict the out-of-plane bending resistance of walls strengthened with SFRM coating.

2. Analytical model formulation

2.1. Shear resistance

As discussed above, the shear failure of coating may be governed either by the formation of diagonal shear cracks or by the attainment of the shear resistance along potential sliding sections occurring, for instance, where the SFRM coating presents discontinuities (e.g., the wall-to-foundation interface). The weakest of these mechanisms governs the total shear resistance (V_R) of masonry. Thus:

$$V_R = \min(V_{R,t}\ ;\ V_{R,s}) \tag{1}$$

where $V_{R,t}$ and $V_{R,s}$ represent the shear resistance related to the diagonal and sliding shear mechanism, respectively.

2.1.1. Diagonal shear resistance

The literature reports different studies focusing on the shear resistance of masonry structures retrofitted by near surface mounted technologies [25,26] as well as FRCM overlays [27]. As suggested by these works, the total in-plane shear capacity of reinforced masonry is obtained by adding two resisting components; the former provided by unreinforced masonry and the second resulting from reinforcement/coating. The rationale behind this assumption is that the total shear resistance of the retrofitted panel can be derived from simple equilibrium considerations, assuming perfect bond between masonry and coating. Likewise reinforced concrete, the potential strain incompatibility between the resisting mechanisms exhibited by masonry and coating are neglected considering that they become progressively less significant as ultimate (i.e., plastic) conditions are approached [28]. Thus, the model proposed herein is based on linear superposition that implicitly considers the internal redistribution of plastic stresses. When dealing with SFRM coating, the plastic stress redistribution generally occurs provided that after cracking the SFRM material is characterized by either a limited softening (i.e., a gradual decrease of resistance) or even a hardening behavior, especially for limited values (<0.5 mm) of the average crack width. Numerical simulations and experiments showed that the latter condition is generally fulfilled when the maximum capacity of the shear wall is attained.

The semi-empirical formulation discussed in the following assumes the total shear to be resisted partly by masonry and partly by coating, by neglecting for simplicity some structural features (e.g., strain compatibility, aggregate interlock forces, dowel action of steel fibers, etc.) that are difficult to assess in practical design. In spite of this, the calibration of the model parameters based on the available numerical and experimental data led to a formulation reliable and quite conservative. However, further verification is needed before using it for design.

When diagonal shear failure of retrofitted masonry occurs, the total shear resistance of the panel ($V_{R,t}$) results from the following semi-empirical equation:

$$V_{R,t} = \min(V_{t,m} + V_{t,coat}\ ;\ V_{R,max}) \tag{2}$$

where $V_{t,m}$ is the shear resistance of URM, $V_{t,coat}$ represents the shear resistance of coating and $V_{R,max}$ is the shear force causing diagonal crushing of masonry [29], i.e.:

$$V_{R,max} = 0.25 \cdot k \cdot f_m \cdot (t_m + n \cdot t_{coat}) \cdot z \tag{3}$$

where:

t_m is the thickness of the masonry panel;

t_{coat} is the thickness of the single SFRM coating layer (see Fig. 1);

f_m is the compressive strength of URM;

$z = 0.8 \cdot L$ is the approximate value of the distance between the resultant of compression and tensile forces (lever arm) acting along the horizontal section of the member;

L is the total length of the wall;

$n = 1, 2$ is the number of coating layers (see Fig. 1).

In the Eq. (3) the factor $k \geq 1$ aims at considering the increase of masonry compressive strength after retrofitting. It can be determined by testing reinforced masonry wallets under uniaxial compression. Otherwise, based on the simple equilibrium of a cross-section in pure

compression, it can be calculated as:

$$k = \frac{t_m + n \cdot t_{coat} \cdot f_c / f_m}{t_m + n \cdot t_{coat}} \quad (4)$$

where f_c is the cylindrical compressive strength of SFRM.

The diagonal shear resistance of URM ($V_{t,m}$) may be predicted by the classical method originally proposed by Turnšek and Cačovic [30] and also reported by the Commentary to the Italian Building Code (clause C8.7.1.16) [31], which considers masonry as an equivalent isotropic material that fails after attaining the tensile strength (f_{mt}):

$$V_{t,m} = L \cdot t_m \cdot \frac{f_{mt}}{b} \cdot \sqrt{1 + \frac{\sigma_0}{f_{mt}}} \quad (5)$$

where:

$\sigma_0 = N/(L \cdot t_m) > 0$ is the average compressive stress acting normally to the URM wall cross-section;

$b = h/L$ is a factor depending on the stress distribution acting over the wall section. It cannot be lower than 1 and higher than 1.5;

h is the height of the wall;

N is the axial compressive force;

$f_{mt} = 1.5\tau_0$ is the tensile strength of URM [21];

τ_0 is the shear strength of URM resulting from a diagonal-compression test.

Note that in case SFRM coating is applied on a pre-damaged (i.e., diagonally cracked) structure, the shear resistance of masonry ($V_{t,m}$) should be considered lower than that resulting from the Eq. (5). Anyway, no analytical formulations are available to estimate the strength reduction of pre-damaged structures and, thus, it should be estimated case-by-case based on the experience or experimental evidences.

As proved by the experimental tests carried out by the Authors of the present paper [13,18], the SFRM coating behaves like a two-dimensional element bonded to the masonry surface. The good bond condition was ensured by a series of steel connectors (4–6 connectors per square meter) that were installed in order to link the coating layer and the wall surface together.

The diagonal failure of SFRM coating is generally preceded by the

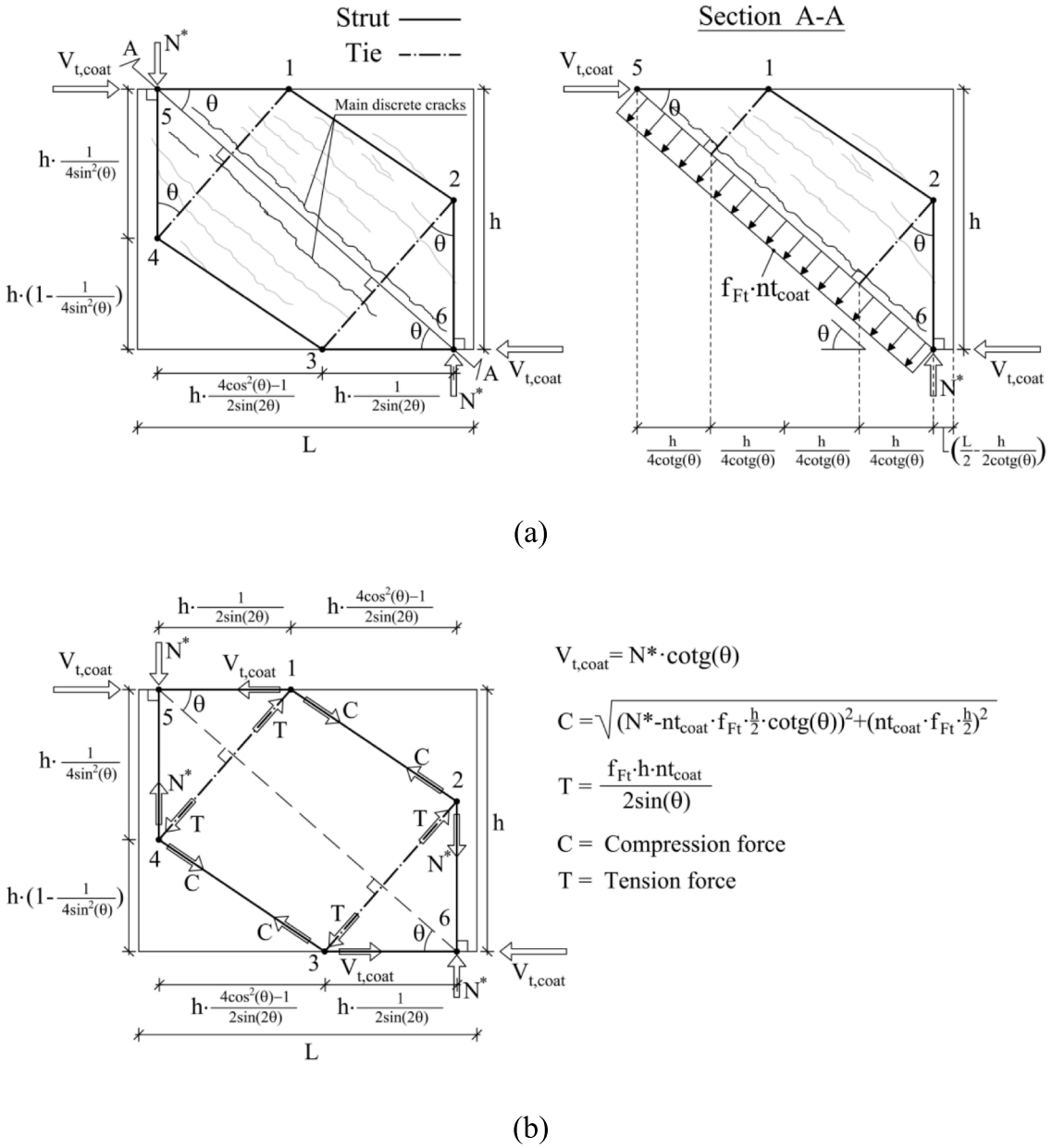

Fig. 2. Diagonal shear resisting mechanism acting in the SFRM coating: (a) Strut-and-Tie schematization and (b) related internal actions.

formation of small cracks smeared over the coating surface, close to the wall diagonal. The number of small cracks developed before failure is closely related to the ability of coating to redistribute internal stresses. In general, the higher the strength and toughness of SFRM, especially for crack widths lower than 0.5 mm, the higher the number of cracks spread over the coating surface. When diagonal failure takes place (Fig. 2a), one or more discrete diagonal cracks may grow. As SFRM is usually made with cementitious composites containing aggregates with a maximum size of about 1 mm, the shear resistance provided by aggregate interlocking [32] is generally negligible. Therefore, the only contribution to the internal resistance after cracking is due to steel fibers. The latter may be represented by a uniform distribution of tensile stresses (f_{Ft}) acting along the discrete diagonal crack/s having the constant slope θ (Fig. 2a).

The SFRM coating behaves like a region subjected to a complex filed of internal stresses. To get insight into the flow of forces acting after cracking, the actual stress field can be represented and reduced to a simple Strut-and-Tie (S&T) model, in which struts and ties represent the compression stress field and the tensile stress contribution provided by the reinforcement (e.g., reinforcing bars and/or steel fibers), respectively. Here, the S&T model consists of six strut elements connected by two ties placed perpendicularly to the fracture plane, i.e. the line connecting the nodes #5 and #6 depicted in Fig. 2b.

The axial force N*, which arises when total shear resistance of coating ($V_{t,coat}$) is achieved, represents the total force resulting from stresses acting along the compressed toe of coating. In more detail, N* is not the total axial force (N) applied on the wall but just the vertical component of the total compression force resisted by the strut located in the SFRM coating. As diagonal shear failure most frequently occurs in double fixed-end walls and piers, the proposed S&T scheme considers the force N* acting in the diagonally-opposite toes of the SFRM panel. The force $V_{t,coat}$ can be computed by the rotation equilibrium of the internal forces acting within the upper half portion of coating (see Section A-A in Fig. 2a). Thus, considering the node #6 of the internal truss as a pivot point, the following equation is obtained:

$$V_{t,coat} = m \cdot f_{Ft} \cdot n \cdot t_{coat} \cdot \frac{h}{2 \cdot \sin^2(\theta)} \tag{6}$$

where:

m = max[1; (2·L/h-1)] is a redundancy factor;

f_{Ft} is the residual tensile strength of SFRM resulting from the Eq. (9);

θ is the average slope of the struts resulting from Eq. (11).

A full description of the parameters f_{Ft} and θ is reported in the following discussion.

The high internal static redundancy of the coating layers together with the increasing aspect ratio of the wall may lead to the activation of a multiple S&T mechanism similar to that represented in Fig. 2. In fact, as numerically observed, squat panels with an aspect ratio L/h higher than 1 tend to develop multiple struts whereas slender panels are generally characterized by the formation of a single strut. To take into account this effect, which allows to increase the energy dissipated by internal inelastic mechanisms, the factor m was included in the Eq. (6).

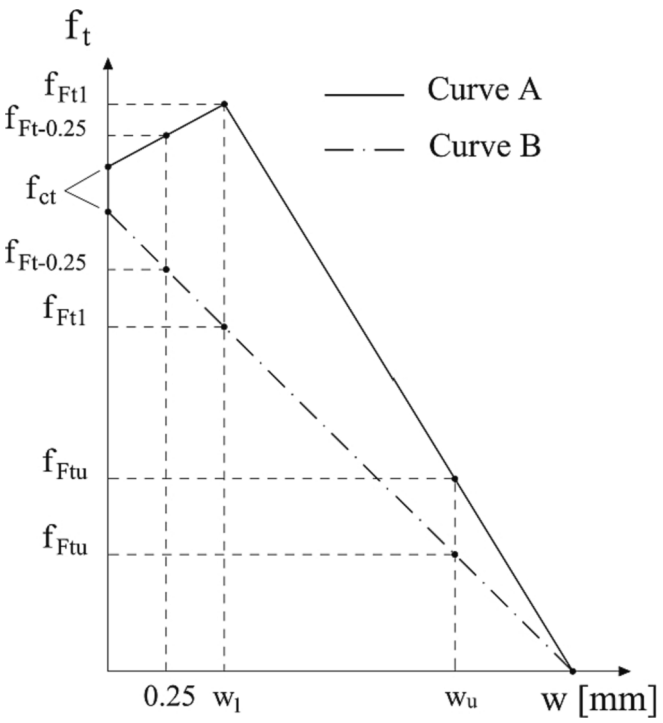

Fig. 3. Typical uniaxial tensile stress (f_t) – crack width (w) law for SFRM.

m herein proposed resulted from a calibration procedure that allowed to minimize the scatter between the analytical predictions of the diagonal shear resistance provided by the Eq. (6) and those obtained from the numerical parametric study described in Section 3.2.

The post-cracking behavior of SFRM can be directly obtained from uniaxial tension tests, from constitutive models reported by codes (e.g., MC2010 [22]) or derived from inverse analysis of either beams or round panel specimens (e.g., see Minelli and Plizzari (2015) [33] and Amin et al. (2017) [34]) subjected to bending. A typical linear uniaxial tensile stress (f_t) – crack width (w) law of SFRM is depicted in Fig. 3. Depending on the SFRM properties (e.g., mechanical performance of the mortar matrix, fiber content, fiber properties, etc.), the constitutive law may exhibit either a full tensile softening behavior (Curve B in Fig. 3) or a hardening response followed by a softening curve (Curve A in Fig. 3).

The linear curve lying between the crack widths w_1 and w_u (Fig. 3) is described by the following relationship:

$$f_t = f_{Ft1} + \frac{f_{Ft1} - f_{Ftu}}{w_1 - w_u} \cdot (w - w_1) \tag{7}$$

where f_t is the stress at crack width w. The residual tensile strength $f_{Ft-0.25}$, corresponding to a crack width of 0.25 mm, can be easily extrapolated from the Eq. (7) as follows:

$$\begin{cases} f_{Ft-0.25} = \dfrac{0.25\text{mm}}{w_1}(f_{Ft1} - f_{ct}) + f_{ct} \quad (CurveA) \quad if\ f_{ct} < 1.25 \cdot f_{Ft1} - 0.25 \cdot f_{Ftu} \\ f_{Ft-0.25} = \dfrac{0.25\text{mm} - w_1}{w_u - w_1}(f_{Ftu} - f_{Ft1}) + f_{Ft1} \quad (CurveB) \quad if\ f_{ct} \geq 1.25 \cdot f_{Ft1} - 0.25 \cdot f_{Ftu} \end{cases} \tag{8}$$

The equation reported above to calculate the factor m resulted from the analysis of the internal stress fields exhibited by the walls analyzed in Section 3. According to the proposed phenomenological interpretation, m represents the potential number of struts acting in the coating as a function of the aspect ratio L/h of the wall. The relation between L/h and

Note that the linear law reported by the MC2010 (clause 5.6.4) [22] for fiber reinforced concrete is very similar to that depicted in Fig. 3, provided that $f_{Ft1} = 0.45 \cdot f_{R1}$, $f_{Ftu} = f_{Ft1} - (w_u/CMOD_3) \cdot (f_{Ft1} - 0.5 f_{R3} + 0.2 f_{R1})$, $w_u = CMOD_3 = 2.5$ mm and $w_1 = 0.5$ mm. Three Point Bending Test (3PBT) carried out according to EN 14651 [35] allows determining

f_{R1} and f_{R3}, which correspond to the residual flexural strengths detected at a Crack Mouth Opening Displacement (CMOD) of 0.5 mm and 2.5 mm, respectively.

Based on the results of the present work as well as on the Authors' experience, the residual strength f_{Ft} may be assumed equal to:

$$f_{Ft} = \max(0.9 \cdot f_{ct} \, ; \, f_{Ft-0.25}) \tag{9}$$

According to the previous equation, when a SFRM with a pronounced tensile softening behavior is adopted, the tensile strength f_{ct} usually governs the shear resistance of coating. On the contrary, when SFRM presents a strain hardening or a slight softening behavior right after cracking, the shear resistance will depend on the residual strength $f_{Ft-0.25}$. The assumption of a crack width of 0.25 mm to determine $f_{Ft-0.25}$ is supported by experimental observations [18] and numerical simulations [36,37] showing that shear failure of strengthened walls generally involves the formation of cracks smaller than 0.2–0.5 mm. In conclusion, Eq. (9) corresponds to a stable or slightly softening behavior of SFRM for small crack widths, thus promoting the internal redistribution of stresses after cracking of coating.

Before cracking, the behavior of the strengthened wall is comparable to that of an elastic 2D continuum subjected to a plane stress condition due to the shear and axial stresses acting in the panel. Considering the uniaxial tensile strength of masonry totally negligible, the cracking condition is attained once the average principal tensile stress achieves the tensile strength of SFRM. Thus, the shear strength (v_{cr}) of the wall at the onset of cracking can be estimated as:

$$v_{cr} = \frac{f_{ct}}{b} \cdot \sqrt{1 + \frac{\sigma_0}{f_{ct}}} \tag{10}$$

where f_{ct} is the uniaxial tensile strength of SFRM whereas $\sigma_0 = N/(L \cdot t_m) > 0$ is the axial stress acting in the URM panel. Eq. (10) includes the same axial stress (σ_0) acting in masonry before retrofitting (see Eq. (5)). This simplifying assumption is made to overcome the difficulties in predicting the actual distribution of the axial stress between masonry and coating. In fact, in real cases, the SFRM overlay is applied on existing buildings when the total gravity and superimposed loads already stress the bearing walls. Therefore, the axial stress acting in the SFRM layer is generally negligible. On the contrary, an increment of the axial stress in the coating is necessarily observed as the lateral load on the wall increases. The axial stress adopted in the Eq. (10) allows to avoid the aforementioned difficulties always leading to a conservative calculation of the total shear resistance resulting from the Eq. (2).

The average slope of the struts is represented by the angle θ determined by the direction of principal compressive stresses acting in the middle of the wall. From the Mohr's circle of stresses of the continuum, one may define the angle θ as follows:

$$\theta = \min\left[\arctan\left(\frac{f_{ct} + \sigma_0}{b \cdot v_{cr}}\right) \; ; \; 90^{\circ}\right] \geq \arctan\left(\frac{h}{L}\right) \tag{11}$$

2.1.2. *Sliding shear resistance*

The increase of the wall resistance after retrofitting may be so high to prevent shear failure due to diagonal compression or tension mechanisms. In this case, after few cycles of lateral displacement reversal, sliding displacements can occur either at the wall base or along flexural cracks, thus forming a continuous and approximately horizontal shear path. To control sliding shear, the shear friction mechanism can be exploited. Along the plane of potential sliding, shear transfer can occur by friction acting in the flexural compression zone. The frictional stress results from the combination of the contributions provided by masonry ($v_{s,m}$) and SFRM coating ($v_{s,coat}$), as shown in the schematic of Fig. 4. Note that the tensile resistance provided by fibers orthogonally tothe cracked section was considered constant and equal to f_{Ft}. When sliding failure takes place, the maximum bending stresses acting in URM (σ_m) and SFRM (σ_{coat}) are usually lower than the corresponding compressive strengths. Moreover, in actual cases, the activation of the sliding mechanism is not necessarily accompanied by the achievement of the maximum flexural capacity. Therefore, in the present work, the length of

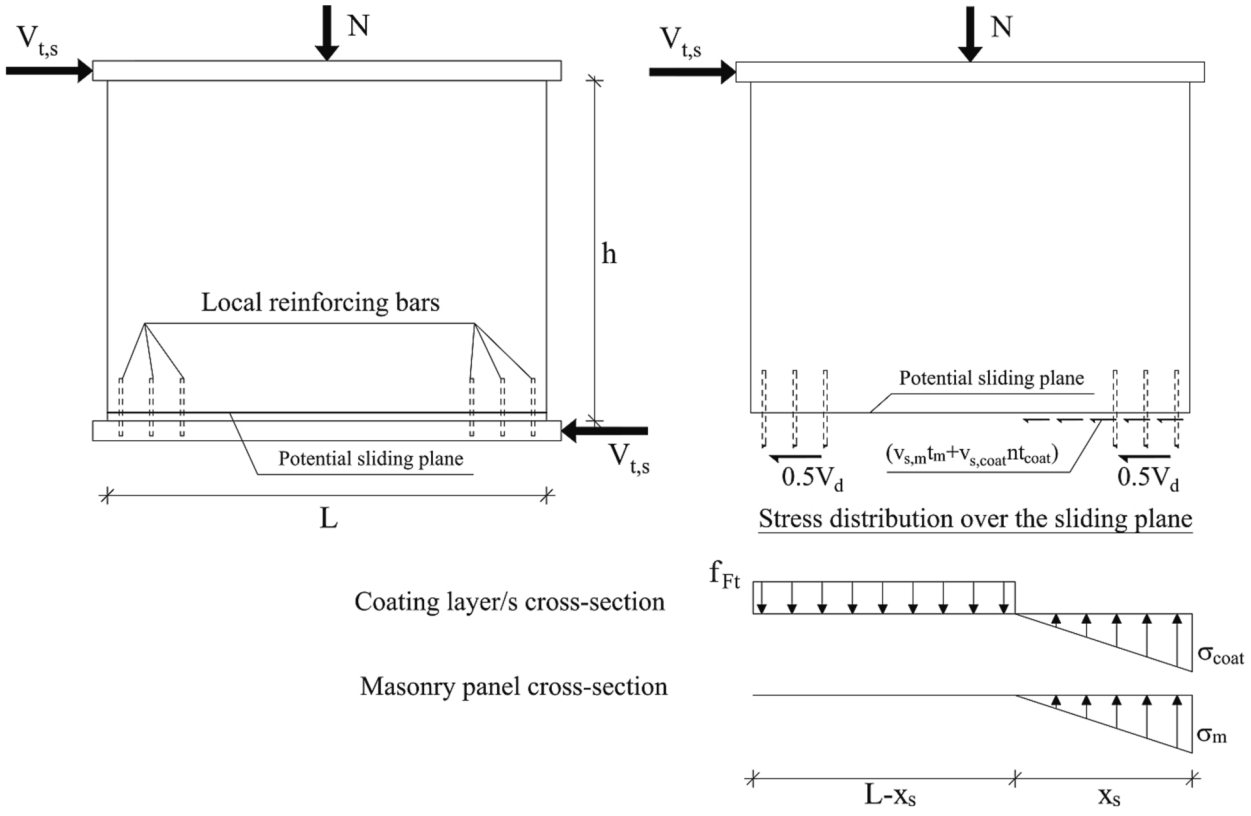

Fig. 4. Shear sliding resisting mechanism acting in the strengthened wall.

the compressed zone (x_s) related to the shear sliding mechanism was different as compared to that calculated for flexural failure (see Section 2.2). As suggested by the Eurocode 6 [23], a linear distribution of the stresses in the compressed zone was assumed.

From the equilibrium, the total resisting force related to the sliding mechanism is equal to:

$$V_{R,s} = x_s \cdot \left(v_{s,coat} \cdot n \cdot t_{coat} + v_{s,m} \cdot t_m\right) + V_d \tag{12}$$

where V_d is the shear resisting force by dowel action of reinforcing bars, if any. The frictional strength of SFRM can be estimated according to the formulation reported by the NTC2018 [21] for concrete walls, which reads as follows:

$$v_{s,coat} = 0.5 \cdot \eta \cdot f_c \tag{13}$$

where:

$\eta = 0.6 \cdot (1\text{-}f_{ck}/250)$ is the strength reduction factor;

f_{ck} is the characteristic compressive strength of SFRM expressed in MPa. According to Eurocode 2 [38], if the mean value of the cylindrical compressive strength (f_{cm}) is known, then the characteristic strength can be estimated as $f_{ck} = f_{cm}$-8 MPa.

As also recommended by the NTC2018 [21], the design sliding shear strength of URM is given by:

$$v_{s,m} = 0.4 \cdot \sigma_{0,s} + f_{v0} \tag{14}$$

in which $\sigma_{0,s} = N/(x_s \cdot t_m)$ and f_{v0} (Table 3) is the sliding shear strength of unit-to-mortar interface at zero compression.

To determine the length x_s, the equilibrium of the potential sliding section subjected to combined flexure and axial compression must be performed. Here, to get a conservative prediction of x_s, the tensile contribution provided by localized rebars (e.g., see Fig. 4) (if any) crossing the sliding section was neglected. The length of the compressed zone results from the following quadratic equation:

$$\frac{1}{6} \cdot x_s^2 \cdot f_{Ft} \cdot n \cdot t_{coat} + x_s \cdot \left[\beta h \cdot \left(v_{s,coat} \cdot n \cdot t_{coat} + f_{v0} \cdot t_m\right) + \frac{1}{3} \cdot f_{Ft} \cdot n \cdot t_{coat} \cdot L + \frac{N}{3}\right] + N \cdot \left(0.4 \cdot \beta h - \frac{L}{2}\right) - \frac{1}{2} \cdot f_{Ft} \cdot n \cdot t_{coat} \cdot L^2 = 0 \tag{15}$$

where βh is the lever arm of the lateral load, with $\beta = 1$ for a cantilever wall and $\beta = 0.5$ for a double fixed-end wall. Note that whether the coating crossing the considered wall section is not continuous, its tensile contribution (i.e., f_{Ft}) in the Eq. (15) must be neglected.

Dowel action of vertical rebars is generally associated with high lateral displacements. The NTC2018 [21] as well as the Eurocode 8 [39] estimate the dowel resistance of vertical bars as follows:

$$V_d = \min \begin{cases} 1.3 \cdot \sum A_{sn} \cdot \sqrt{f_c \cdot f_y} \\ 0.25 \cdot f_y \cdot \sum A_{sn} \end{cases} \tag{16}$$

where:

$\sum A_{sn}$ is the sum of the areas of the vertical bars crossing the potential sliding section;

f_y is the yielding strength of vertical rebars.

2.2. Flexural resistance

To calculate the flexural resistance of the cross-section of a retrofitted wall, the stress and strain distribution shown in the schematic of Fig. 5 can be adopted. Symmetrical vertical reinforcing bars at both ends were included in the calculation to consider the resisting contribution of localized conventional reinforcement, if any. As discussed by the Authors in a previous work [18], vertical short rebars placed within the coating thickness can be used to increase the bending resistance of the wall especially where the SFRM coating presents discontinuities (e.g. the wall-to-foundation interface), which are not able to withstand tensile stresses acting normally to the sliding plane. Since perfect bond between masonry and coating was assumed (i.e., no relative slip at the masonry-to-coating interface; no detachment of coating from the masonry surface), the following classical hypotheses can be stated in order to derive a general formulation for the flexural resistance. 1) Plane sections remain plane after bending (Bernoulli's principle). 2) An elastic–plastic constitutive law is assumed for reinforcing steel. 3) Tensile strength of masonry is neglected. 4) Post-cracking tensile strength of SFRM is taken into account provided that no discontinuities are located along the cross-section plane. In this latter case the tensile contribution of fibers must be neglected. 5) A constant distribution of stresses (stress-block) acting along the cross-section is assumed both for masonry (i.e. Eurocode 6 [23]) and SFRM (i.e. MC2010 [22]) in compression. About the tensile stresses acting in the SFRM, the rigid-plastic model recommended by the MC2010 [22] was adopted.

The same strain distribution (Fig. 5) was assigned to both masonry and SFRM, which assumes an ultimate strain (ε_c) at the extreme

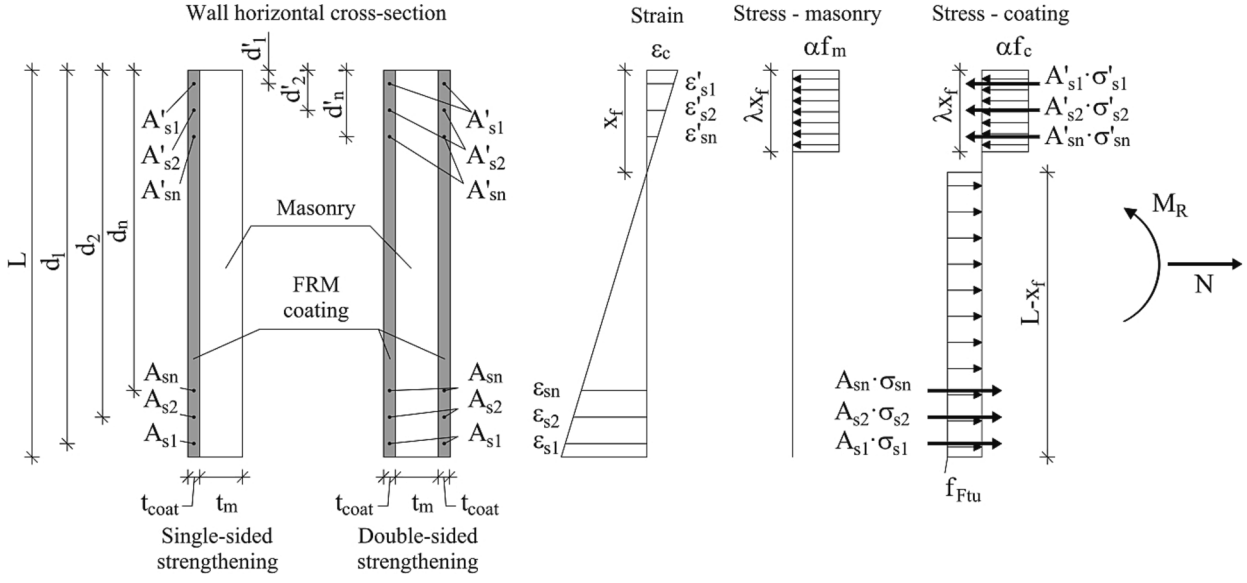

Fig. 5. Stress and strain distribution acting over a wall cross-section subjected to bending.

compression fiber equal to 3.5 ‰. The adopted compressive stress distribution (stress-block) is consistent with that suggested by the Italian code [21] as well as by European standards [23,38,22]. A rigid-plastic model with a constant strength was used to represent the tensile behavior of SFRM according to MC2010 [22]. As stated above, the tensile contribution of coating (f_{Ftu}) must be neglected along those sections presenting discontinuities such as, for example, the interface between the wall and the foundation or between the internal SFRM layer and the floor slab in case of double-sided strengthening.

The depth (x_f) of the stress block must be first calculated from the equilibrium of axial forces. Thus, the following equation is obtained:

$$N = \alpha\cdot\lambda\cdot x_f\cdot(f_m\cdot t_m + f_c\cdot n\cdot t_{coat}) - f_{Ftu}\cdot n\cdot t_{coat}\cdot(L - x_f) + \sum_{1}^{n}(A'_{sn}\cdot\sigma'_{sn} - A_{sn}\cdot\sigma_{sn}) \quad (17)$$

where:

A_{sn} is the total area of the n^{th} vertical rebar placed in the tensile zone;

A'_{sn} is the total area of the n^{th} vertical rebar placed in the compressed zone;

$\sigma_{sn} = \min(f_y; \varepsilon_{sn}\cdot E_s)$ is the stress acting in the n^{th} tensile vertical rebar;

$\sigma'_{sn} = \min(f_y; \varepsilon'_{sn}\cdot E_s)$ is the stress acting in the n^{th} compressed vertical rebar;

E_s is the Young's modulus of reinforcing steel;

ε_{sn}, ε'_{sn} are the strains acting in the tensile and compressed rebars, respectively;

x_f is the depth of the neutral axis;

$\lambda = 0.8$ is the factor defining the effective height of the compressed zone of masonry [23] and SFRM [22];

$\alpha = 0.85$ is the coefficient taking into account the long term effects on the compressive strength according to the NTC2018 [21].

According to EN14651 [35], the ultimate tensile strength f_{Ftu} can be assumed equal to $f_{R3}/3$ (f_{R3} = residual flexural strength corresponding to a crack width of 2.5 mm) as required by the rigid-plastic model defined by the MC2010 [22]. Experimental observations [18] and numerical simulations have shown that this assumption is, in most of the cases, reasonably conservative. In fact, walls retrofitted by SFRM coating generally exhibit flexural cracks at failure with maximum widths higher

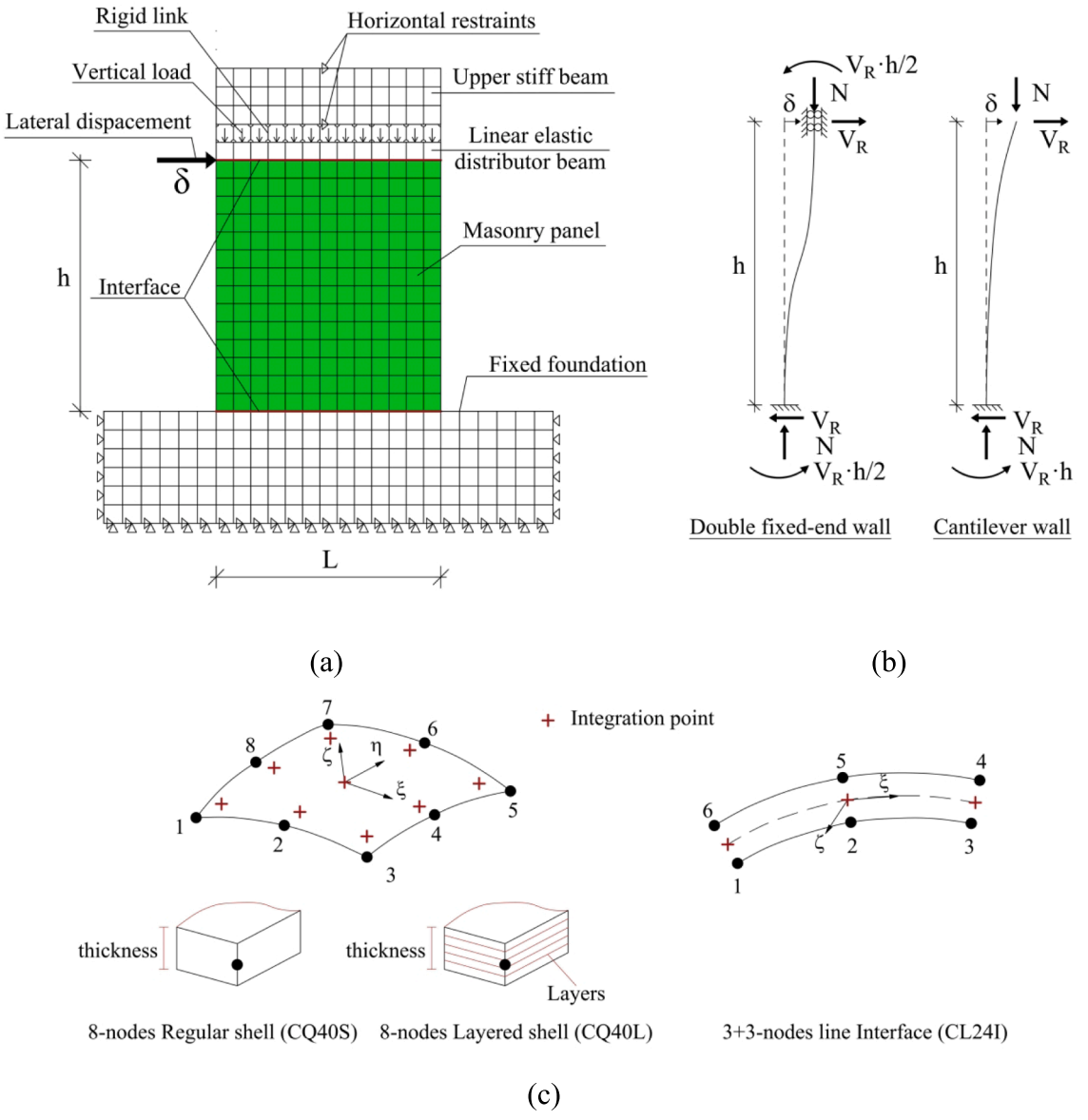

Fig. 6. (a) Typical FE model of the wall. (b) Boundary conditions considered in the parametric study. (c) Schematic of the isoparametric elements adapted from [41].

than 2 mm.

The resisting moment (M_R) can be evaluated as follows:

$$M_R = -\frac{\alpha\cdot(f_m\cdot t_m + f_c\cdot n\cdot t_{coat})\cdot(\lambda\cdot x_f)^2}{2} + \frac{f_{Ftu}\cdot\left(L^2 - x_f^2\right)}{2}\cdot n\cdot t_{coat} + \sum_1^n (A_{sn}\cdot\sigma_{sn}\cdot d_n - A'_{sn}\cdot\sigma'_{sn}\cdot d'_n) + \frac{N\cdot L}{2} \quad (18)$$

where d_n and d'_n are the effective depths of tensile and compressed rebars, respectively. Note that the reinforcement is symmetrically placed within the section as suggested in a previous work [18].

Moreover, it should be noted that, if SFRM coating and conventional reinforcement are not used, Eq. (18) reduces to that recommended by NTC2018 (clause 7.8.2) [21] and EN 1998–3 (clause C4.2) [40] for URM sections.

3. Model validation

Because of the limited experimental data currently available [13,17,18,36], the analytical model was mainly validated against the results of a parametric study based on non-linear numerical simulations. The parametric study considered walls having different material (i.e., masonry and SFRM) and geometrical properties (e.g., wall thickness, coating thickness, wall aspect ratio, etc.) in order to have a broad perspective on the actual effectiveness of the proposed analytical model.

The Finite Element (FE) program Diana 10.4 [41] was used to perform the numerical analyses. As shown in a previous work [17], the constitutive models implemented in the Diana 10.4 code for quasi-brittle materials are effective in predicting the response of both single members and buildings strengthened with SFRM coating.

The typical FE model of the walls used in the parametric study is shown in Fig. 6a. It adopts 8-nodes isoparametric curved shell elements (Fig. 6c) with a 3x3 Gaussian integration scheme in the plane of the element and a 5-points Simpson scheme in the thickness direction. Preliminary sensitivity simulations of the analyzed walls showed that the adoption of shell elements with dimensions of about 100x100 mm provided a mesh refinement able to accurately predict the member response. Two different shell element typologies are available in the program, namely the regular and the layered element, respectively (Fig. 6c). Unlike the regular elements, the thickness of the layered shell is subdivided into a number of layers that may have different material and thickness properties. Further details about the element formulation can be found in [41]. URM walls with uniform properties over the thickness can be modelled by regular shell elements. On the contrary, the layered shells are suitable for simulating laminated elements with variable properties over the thickness, such as the walls strengthened with SFRM coating.

To model potential sliding mechanisms occurring at the top or the bottom side of the wall, 3 + 3 nodes isoparametric line interface elements (Fig. 6c) were used to connect the masonry panel with both the foundation and the distributor beam (Fig. 6a). A 3-points Newton-Cotes integration scheme was adopted in the isoparametric direction ξ whereas a 5-points Simpson scheme was selected for the integration in the thickness direction.

Both double fixed-end and cantilever walls were analyzed in the parametric study (Fig. 6b). To represent the double fixed-end condition, the base side of the masonry panel was rigidly connected to a large stiff foundation (Fig. 6a). On the contrary, the upper side of the wall was free to translate whereas the rotation about the transversal axis (i.e., z axis) was restrained. The latter condition was obtained by joining together the stiff distributor beam located at the top of the masonry panel (i.e., the "Linear elastic distributor beam") and the "Upper stiff beam" by vertical rigid links. Note that the ability of the "Upper stiff beam" to freely translate vertically allows to keep the axial load constant as the masonry panel is laterally displaced. To simulate the cantilever wall, the top stiff beam and the link elements were both removed from the model.

The behavior of masonry and SFRM was simulated by a smeared crack model (i.e., "total strain rotating crack model" [41]), in which the constitutive stress–strain relationships are evaluated in the principal direction of the strain vector.

About masonry, the parabolic constitutive law proposed by Feenstra [42] was used to simulate the stress–strain behavior in compression. As shown in the schematic of Fig. 7a, the law depends on the compressive strength (f_m) and the compressive fracture energy (G_c). Based on the tensile strength ($f_{mt,num}$) and the mode-I tensile fracture energy (G_f^I), the Hordijk's [43] law was adopted to model the post-cracking behavior of URM, whereas a simple tensile linear stress–strain curve was implemented to describe the elastic response in the pre-cracked stage.

The compressive behavior of SFRM was represented by the Thorenfeldt's model [44] (Fig. 7b), whose formulation depends only on the compressive strength (f_c). A linear elastic law with constant elastic modulus (E) governed the tensile behavior up to the achievement of the tensile strength (f_{ct}). After cracking, the multilinear stress-crack width law shown in Fig. 3 was implemented.

To make the energy dissipated during failure independent from the numerical discretization, a proper characteristic length must be incorporated in the continuum equations. As proposed by Rots [45], the mesh objectivity is restored by using a characteristic length (h_{ch}) depending on the size of the finite element (i.e., $h_{ch} = A^{1/2}$, A = area of the single shell element).

To model the frictional behavior of the interface located along the top and bottom side of the masonry panel, a non-linear elastic friction

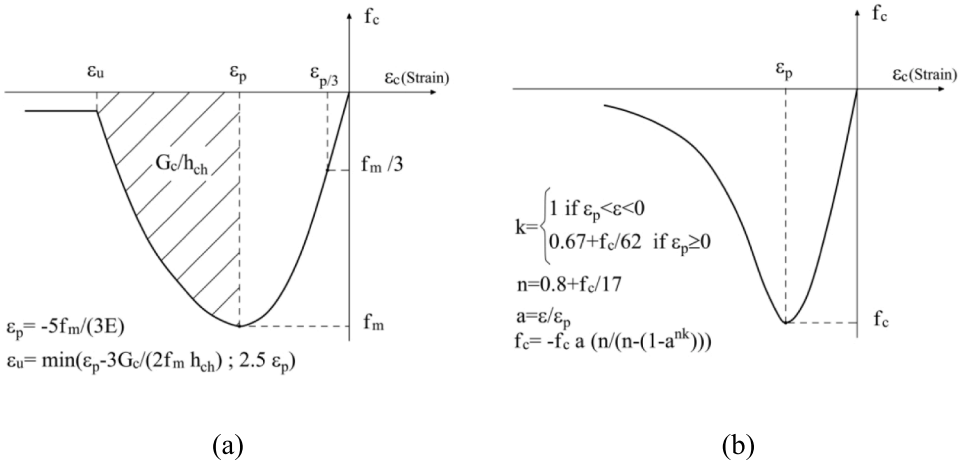

Fig. 7. Material constitutive laws in compression for (a) URM and (b) SFRM.

model was implemented. The variables that define the behavior of the structural interface are oriented in the local x-y-z reference system (Fig. 6c). The interface model is defined by the generalized strain (**u**) and stress (**f**) vectors. The former $\mathbf{u} = [u_{sx}, u_{ny}, u_{sz}]^T$ consists of the relative shearing (u_{sx}, u_{sz}) and normal (u_{ny}) displacement components. The latter $\mathbf{f} = [f_{sx}, f_{ny}, f_{sz}]^T$ consists of the shear traction components f_{sx} and f_{sz} acting parallel to the x- and z- local axes as well as by the normal traction f_{ny} parallel to the y-axis. In the elastic stage, the behavior of the interface is governed by the equation $\mathbf{f} = \mathbf{D^e}\,\mathbf{u}$, where $\mathbf{D^e} = \text{diag}\,[k_{sx}, k_{ny}, k_{sz}]$ represents the elastic stiffness matrix. The effective shear stress $\tau = (f_{sx}^2 + f_{sz}^2)^{1/2}$ is related to the normal stress by the yield function $|\tau| + f_{ny}\cdot\tan(\phi) - c = 0$ depending on the friction angle ϕ and the cohesion c. Since the interface was included in the FE model to represent the shear-sliding mechanism considered by the proposed analytical model (see par. 2.1.2), the parameter $\tan(\phi)$ was assumed equal to 0.4 to be consistent with the friction angle recommended by NTC2018. Assuming that the thickness of the interface element is t_m, the cohesion can be computed as the combination of the contributions of masonry and coating according to the equation $c = 0.5\cdot\eta\cdot f_c\cdot t_{coat}/t_m + f_{v0}$. In the elastic regime the deformation of the interface was considered negligible and, thus, the normal and tangent elastic stiffnesses (k_{sx}, k_{ny}, k_{sz}) were all set equal to $1x10^8$ N/mm^3.

All the simulations were performed under lateral deflection (δ) control and a constant axial load (N) uniformly distributed along the top side of the masonry panel. A regular Newton-Raphson iteration scheme was adopted, with a line search algorithm improving the method's robustness. To check convergence of the iteration process, the force and displacement norms were both controlled by setting the corresponding tolerances ≤ 0.01.

3.1. Validation of the numerical model

Table 1 summarizes the main properties of five URM shear walls reported by the literature [46–49,36] and here used as reference samples for the parametric study. The compressive strength (f_m) and the elastic modulus (E) of masonry were determined from the data reported in the aforementioned experimental works, whereas the remaining mechanical parameters (i.e., ν, $f_{mt,num}$, G_c and G_f^I) were calibrated so that the numerical response provided the best prediction of the load–deflection curves observed in the experimental tests. The results of Table 1 highlight the good accuracy of the numerical model that provided total base shear values (V_R^{num}) very close (i.e., $V_R^{num}/V_R^{exp} = 1.02$ on average) to the experimental ones (V_R^{exp}). As occurred in the experimental tests, all the reference walls attained the maximum capacity after exhibiting a diagonal shear mechanism.

Two different experimental case studies were considered.

The former considers two full-scale cantilever walls, hereafter named as wall #66 and wall #67, which were tested at the University of Brescia. As discussed in [36], the specimens had a total length of 3000 mm, a height of 1970 mm and were made with the hollow-block masonry material MAS5 described in Table 1. Moreover, the total thickness of the walls #66 and #67 URM was respectively 240 mm and 200 mm. Both sides of the walls were strengthened with a 25 mm thick coating made with the fiber reinforced mortar SFRM7 (see Table 2). Unlike the wall #66, the wall #67 was provided with vertical 8 mm diameter steel rebars located on each side of the element to connect the coating layer to the concrete foundation of the specimen. As shown in the schematic of Fig. 8a, the rebars were located in the middle of the coating thickness and fixed to the foundation by epoxy grout injected into pre-drilled holes. The walls were tested under a constant axial load (N) of 250 kN and horizontal reverse cycling loading. The experimental results showed that the increase of the shear resistance due to retrofitting allowed to turn the diagonal shear failure mechanism of the URM walls into the flexural mode exhibited by the retrofitted ones. For the sake of example, the crack pattern at failure of the wall #67 has been represented in Fig. 8b. The maximum lateral resistance of the test wall #66 was 202 kN whereas the wall #67 attained a higher flexural capacity (i.e., 316 kN) due to the contribution to flexural resistance provided by the coating-to-foundation anchor rebars.

The FE simulations of the two walls were performed in a monotonic fashion by adopting the model discussed at the beginning of this Section. The response of the wall #66 was well captured by the numerical model, which provided a maximum lateral capacity (i.e., 214 kN) 6 % higher than the actual one. A reasonably good prediction was also obtained for the wall #67, since the numerical maximum capacity (i.e., 312 kN) was only 1 % lower than the experimental one (i.e., 316 KN). This good result was obtained by reducing the tensile strength of rebars to 218 MPa in order to account for splitting failure observed in the experimental test (see Section 3.2, Eq. (20)). The flexural failure modes experienced by both test walls were consistent with those obtained from the simulations.

The second case study considers a 5.75x4.25x6.7 (height) m two-story full-scale masonry building tested at the University of Brescia under quasi-static reverse cyclic loading. The structure was retrofitted by a 30 mm thick layer of SFRM coating applied only on the outer surface of the walls. All the details concerning the experimental test can be found in [18]. The main results of the experimental test have been compared with those provided by the 3-D FE simulation of the building based on the "smeared crack model" described above. The model implemented the mechanical properties herein referred to as MAS5 (Table 1) and SFRM1 (Table 2) respectively for URM and SFRM. A comprehensive description of the numerical analysis is reported in [36,37]. Here only the total base shear (V_b) – top deflection (δ) response and the numerical crack patterns were compared with the corresponding experimental ones. As shown in Fig. 9a, the numerical model was able to well capture both the pre-peak lateral stiffness and the maximum capacity of the building. The numerical and the experimental crack-patterns at peak load are compared in Fig. 9b. As it can be observed, the flexural and the diagonal shear cracks affecting the piers of the ground story were consistent with the post-cracking strains reported in the numerical contours. These good results further confirm the ability of the FE model to predict all the most significant mechanisms presented by retrofitted masonry, including those involving shear-critical structural elements.

Table 1
Properties considered in the numerical analysis of the URM test walls.

Wall ID	Ref.	URM ID	Wall restr.[1]	N [kN]	L [m]	h [m]	t_m [mm]	ν [-]	E [MPa]	$f_{mt,num}$ [MPa]	f_m [MPa]	G_c [N/mm]	G_f^I [N/mm]	V_R^{exp} [kN]	V_R^{num} [kN]	$\frac{V_R^{num}}{V_R^{exp}}$
CT02	[46]	MAS1	DF-W	160	2.50	2.50	320	0.2	800	0.13	3.28	5.3	0.001	140	143	1.02
WIVb	[47]	MAS2	DF-W	205	1.36	0.90	236	0.2	1300	0.24	4.53	10.0	0.10	158	163	1.03
RDB-01	[48]	MAS3	DF-W	300	2.50	2.00	300	0.2	700	0.15	2.33	50.0	0.01	156	162	1.04
PUP1	[49]	MAS4	DF-W	418	2.01	2.23	200	0.2	2500	0.08	5.87	10.0	0.10	175	170	0.97
MW3	[36]	MAS5	C-W	250	3.00	1.97	200	0.2	2100	0.05	2.30	3.0	0.01	128	132	1.03
															Mean [-]	1.02
															CV [%]	2.7

[1] Wall restraints: C-W = cantilever wall; DF-W = double fixed-end wall.

Table 2
Properties of SFRM used in the numerical simulations and in the analytical model.

SFRM ID	E [MPa]	f_c [MPa]	f_{ct} [MPa]	$f_{Ft-0.25}$ [MPa]	f_{Ft1} [MPa]	w_1 [mm]	f_{Ftu} [MPa]	w_u [mm]
SFRM1	21,000	36	2.00	2.16	2.50	0.8	1.80	2.5
SFRM2	21,000	18	2.00	2.16	2.50	0.8	1.80	2.5
SFRM3	21,000	36	2.00	1.65	1.30	0.5	0.57	2.5
SFRM4	21,000	36	3.00	1.65	0.30	0.5	0.10	2.5
SFRM5	30,000	36	2.00	1.65	1.30	0.5	0.57	2.5
SFRM6	21,000	25	3.00	1.77	0.54	0.5	0.10	2.5
SFRM7	14,400	25	1.65	1.68	1.70	0.5	1.25	2.5

Table 3
Shear strength of URM and shear resistance calculated by Eq. (5).

Wall ID	URM ID	N [kN]	L [m]	b [-]	t_m [mm]	f_{v0} [MPa]	f_{mt} [MPa]	$V_{t,m}$ [kN]	V_R^{exp} [kN]	$\frac{V_{tm}}{V_R^{exp}}$
CT02	MAS1	160	2.50	1.0	320	0.10[1]	0.11	148	140	1.06
WIVb	MAS2	205	1.36	1.0	236	0.39[2]	0.27	159	158	1.01
RDB-01	MAS3	300	2.50	1.0	300	0.25[2]	0.09	158	156	1.01
PUP1	MAS4	418	2.01	1.1	200	0.27[2]	0.19	176	175	1.01
MW3	MAS5	250	3.00	1.0	200	0.20[3]	0.09	128	128	1.00
									Mean [-]	1.01
									CV [%]	0.81

[1] Minimum mean value recommended by [31] for stone masonry with a regular pattern.
[2] Mean value reported by the Author of the experimental test.
[3] Minimum mean value recommended by [31] for hollow-block masonry.

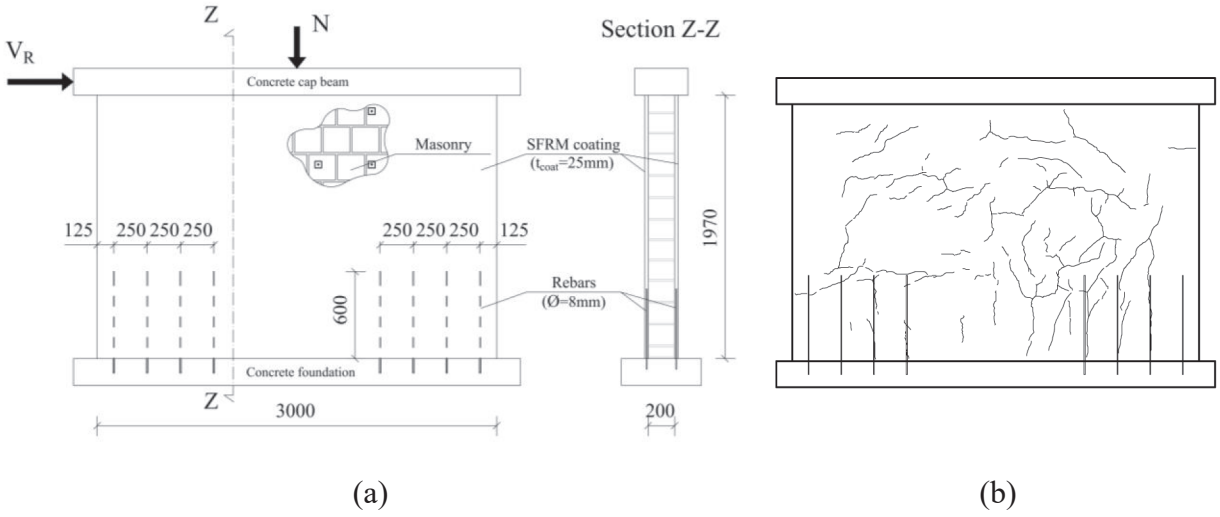

Fig. 8. (a) Wall #67 details and (b) experimental crack pattern at failure. (dimensions in mm).

The numerical simulation of the building allowed to calculate the maximum resistance of the central pier "P7" (see Fig. 9b – ground story), which will be hereafter named as wall #68. This wall failed under diagonal shear after attaining a maximum resistance of 126 kN. To calculate this resistance, the shear stresses acting along the bottom side of the pier were integrated over the entire wall width (i.e., 1250 mm). The integration procedure was repeated for every step of the numerical simulation until the maximum shear capacity of the pier was found. As discussed in Section 3.2, this value of capacity was compared with that provided by the proposed analytical model to further enhance its validation.

3.2. Validation of the proposed analytical model

The five walls described in the previous section were used as reference samples to perform a parametric study aiming at simulating strengthening arrangements characterized by different SFRM properties, coating thickness, number of strengthened sides, wall aspect ratios and axial loads (Table 4).

Regarding the material properties, the parametric analysis considered the masonry materials (i.e., MAS1-5) summarized in Table 1 and the seven SFRM materials (i.e., SFRM1-7) described in Table 2. The SFRM materials are characterized by different compressive strengths and tensile properties, being these latter represented by the tensile strength and crack width parameters defining the multilinear law depicted in Fig. 3. Note that the properties of SFRM1, SFRM2 and SFRM7 are typical of materials having a strain-hardening behavior after cracking. On the opposite, the materials SFRM3-5 present a typical softening behavior after cracking.

The analytical prediction of the diagonal shear strength of the URM test walls is based on the equation proposed by Turnšek and Cačovic [30]. As shown by other authors [50], the accuracy of this equation is mainly dependent on the value of the masonry diagonal tensile strength (f_{mt}), which is not necessarily coincident with the tensile strength (i.e.,

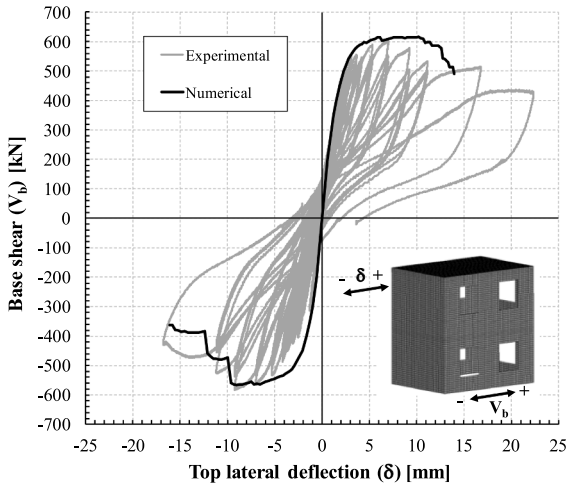

(a)

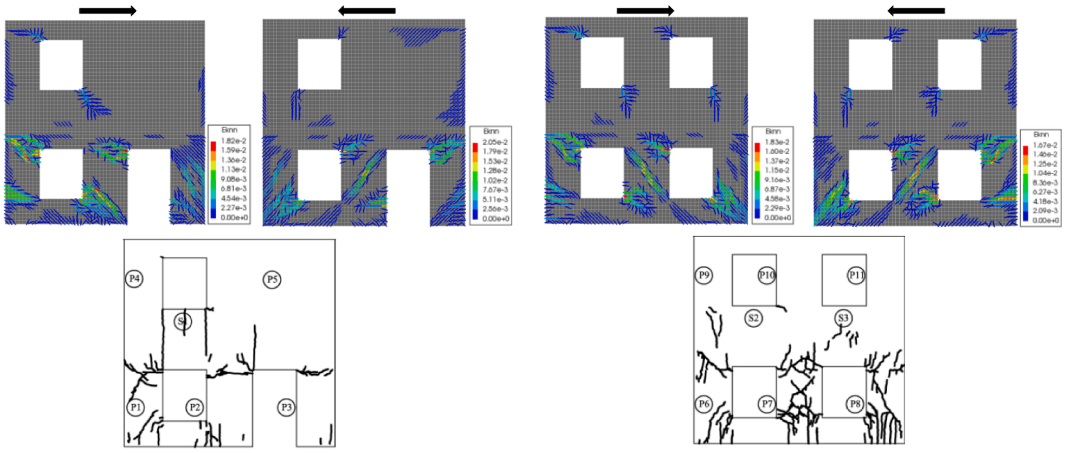

(b)

Fig. 9. Comparison between the experimental and the numerical response of the test building [36] retrofitted with SFRM coating: (a) total base shear (V_b) vs top deflection (δ) response; (b) crack pattern at the maximum base shear.

$f_{mt,num}$ - Table 1) resulting from the numerical calibration. Therefore, a further calibration procedure was performed to determine the tensile strength that must be implemented in Eq. (5) to get a shear resistance as close as possible to the capacity (V_R^{exp}) of the test walls. The resulting values of the tensile strengths implemented in the analytical model are reported in Table 3 together with the comparison between the experimental capacity (V_R^{exp}) and the one ($V_{t,m}$) calculated by the Eq. (5).

The parametric study involved a total of 68 cantilever or double fixed-end walls, three of which were also investigated by experimental tests performed at the University of Brescia. Table 4 summarizes the properties of each wall as well as the total lateral resistances (V_R) resulting from both the numerical simulation (V_R^{num}) and the analytical prediction (V_R^{an}) obtained from the proposed analytical model. When considering the analytical prediction, V_R was calculated as the minimum of the four components related respectively to the maximum shear strength ($V_{R,max}$), the diagonal shear failure ($V_{R,t}$), the sliding shear failure ($V_{R,s}$) and the flexural failure ($V_{R,flex}$). For the sake of clarity, a step-by-step description of the procedure used to implement the analytical model is shown in the worked example reported in Section 4.

The failure mode predicted by the proposed model was consistent with the numerical one for 58 of the 68 walls included in Table 4. As highlighted by the diagram of Fig. 10, the relatively low value of the MAPE (11.7 %) proves the good accuracy of the analytical model. The inaccuracy of the model seems to increase as the aspect ratio (h/L) decreases to values lower than 0.5. However, the analytical predictions are, in most of the cases, more conservative than the results of the numerical simulations. About the wall #66 and #67, the evaluation of the flexural resistance by the proposed model was made without considering the tensile strength (f_{Ft}) of SFRM, since the coating was not connected to the wall foundation. Furthermore, the prediction of the lateral resistance of wall #67 required to take into account the contribution of vertical reinforcement. The latter was provided with a small clear cover (8.5 mm) that promoted the formation of vertical splitting cracks running parallel to each rebar (Fig. 8b). The bond strength for splitting failure can be estimated by the following equation reported by the MC2010 (clause 6.1.1.1) [22]:

$$\tau_{bu,split} = \eta_2 \cdot 6.5 \cdot \left(\frac{f_{cm}}{25}\right)^{0.25} \cdot \left(\frac{25}{\varnothing}\right)^{0.2} \cdot \left[\left(\frac{c_{min}}{\varnothing}\right)^{0.33} \cdot \left(\frac{c_{max}}{c_{min}}\right)^{0.1}\right] = 10.9\,\text{MPa} \quad (19)$$

where:

$\eta_2 = 1$ for good bond conditions;

$f_{cm} = f_c = 25$ MPa is the mean compressive strength of mortar SFRM7;

Table 4
Results of the parametric study.

											Proposed analytical model									Numerical		
Ref. #	URM ID	Wall restr.[1]	L [m]	h [m]	h/L [-]	t_m [mm]	t_{coat} [mm]	n [-]	N [kN]	SFRM ID	x_f [mm]	x_s [mm]	θ [°]	$V_{R,max}$ [kN]	$V_{R,flex}$[2] [kN]	$V_{R,t}$ [kN]	$V_{R,s}$ [kN]	V_R^{an} [kN]	Fail. mode[3]	V_R^{num} [kN]	Fail. mode[3]	$\frac{V_R^{an}}{V_R^{num}}$
1	MAS1	DF-W	2.50	2.50	1.00	320	30	1	160	SFRM1	168	628	46	1065	279	302	265	265	S	290	F	0.91
2	MAS1	DF-W	2.50	2.50	1.00	320	15	2	160	SFRM1	168	628	46	1065	279	302	265	265	S	286	F	0.93
3	MAS1	DF-W	2.50	2.50	1.00	320	15	1	160	SFRM1	175	728	46	795	215	225	192	192	S	215	F	0.89
4	MAS1	DF-W	2.50	2.50	1.00	320	15	2	160	SFRM2	223	917	46	795	274	302	236	236	S	278	F	0.85
5	MAS1	DF-W	2.50	2.50	1.00	320	30	1	160	SFRM3	118	574	46	1065	195	277	247	195	F	224	F	0.87
6	MAS1	DF-W	2.50	2.50	1.00	320	15	2	160	SFRM3	118	574	46	1065	195	277	247	195	F	225	F	0.87
7	MAS1	DF-W	2.50	2.50	1.00	320	30	1	400	SFRM1	304	843	48	1065	482	353	430	353	D	371	D	0.95
8	MAS1	DF-W	2.50	2.50	1.00	320	15	2	400	SFRM1	304	843	48	1065	482	353	430	353	D	387	D	0.91
9	MAS1	DF-W	2.50	2.50	1.00	320	15	1	400	SFRM1	360	1040	48	795	413	280	343	280	D	283	D	0.99
10	MAS1	DF-W	2.50	2.50	1.00	320	15	2	400	SFRM2	404	1157	48	795	465	353	377	353	D	377	D	0.94
11	MAS1	DF-W	2.50	2.50	1.00	320	30	1	400	SFRM3	257	801	48	1065	406	329	416	329	D	353	D	0.93
12	MAS1	DF-W	2.50	2.50	1.00	320	15	2	400	SFRM3	257	801	48	1065	406	329	416	329	D	390	D	0.84
13	MAS1	DF-W	1.25	2.50	2.00	320	30	1	200	SFRM1	152	153	63	532	121	170	129	121	F	131	F	0.92
14	MAS1	DF-W	1.25	2.50	2.00	320	15	2	200	SFRM1	152	153	63	532	121	170	129	121	F	132	F	0.91
15	MAS1	DF-W	1.25	2.50	2.00	320	30	1	200	SFRM3	129	137	63	532	102	153	124	102	F	118	F	0.86
16	MAS1	DF-W	1.25	2.50	2.00	320	15	2	200	SFRM3	129	137	63	532	102	153	124	102	F	119	F	0.85
17	MAS1	DF-W	4.00	2.50	0.63	320	30	1	256	SFRM1	269	1535	46	1704	714	577	593	577	D	537	D	1.07
18	MAS1	DF-W	4.00	2.50	0.63	320	15	2	256	SFRM1	269	1535	46	1704	714	577	593	577	D	552	D	1.04
19	MAS1	DF-W	5.00	2.50	0.50	320	30	1	320	SFRM1	336	2270	46	2130	1116	759	854	759	D	733	D	1.04
20	MAS1	DF-W	5.00	2.50	0.50	320	15	2	320	SFRM1	336	2270	46	2130	1116	759	854	759	D	751	D	1.01
21	MAS1	DF-W	4.00	2.50	0.63	320	30	1	256	SFRM3	189	1432	46	1704	499	520	560	499	F	508	D	0.98
22	MAS1	DF-W	4.00	2.50	0.63	320	15	2	256	SFRM3	189	1432	46	1704	499	520	560	499	F	508	D	0.98
23	MAS1	DF-W	5.00	2.50	0.50	320	30	1	320	SFRM3	236	2136	46	2130	780	682	811	682	D	686	D	0.99
24	MAS1	DF-W	5.00	2.50	0.50	320	15	2	320	SFRM3	236	2136	46	2130	780	682	811	682	D	624	D	1.09
25	MAS2	DF-W	1.36	0.90	0.66	236	30	1	205	SFRM1	157	591	49	585	382	263	307	263	D	268	D	0.98
26	MAS2	DF-W	1.36	0.90	0.66	236	15	2	205	SFRM1	157	591	49	585	382	263	307	263	D	270	D	0.97
27	MAS2	DF-W	1.36	0.90	0.66	236	15	1	205	SFRM1	184	687	49	438	326	211	244	211	D	216	D	0.98
28	MAS2	DF-W	1.36	0.90	0.66	236	30	1	205	SFRM3	132	568	49	585	319	245	298	245	D	246	D	1.00
29	MAS2	DF-W	1.36	0.90	0.66	236	15	2	205	SFRM3	132	568	49	585	319	245	298	245	D	247	D	0.99
30	MAS3	DF-W	5.00	2.00	0.40	300	30	1	150	SFRM1	284	2072	46	1779	1002	702	811	702	D	627	D	1.12
31	MAS3	DF-W	5.00	2.00	0.40	300	15	2	150	SFRM1	284	2072	46	1779	1002	702	811	702	D	606	D	1.16
32	MAS3	DF-W	5.00	2.00	0.40	300	30	1	525	SFRM1	538	2828	47	1779	1815	778	1236	778	D	948	D	0.82
33	MAS3	DF-W	2.50	2.00	0.80	300	30	1	300	SFRM4	216	936	47	890	358	386	460	358	F	318	F	1.13
34	MAS3	DF-W	2.50	2.00	0.80	300	15	2	300	SFRM4	216	936	47	890	358	386	460	358	F	318	F	1.13
35	MAS3	DF-W	2.50	2.00	0.80	300	15	1	300	SFRM4	306	1061	47	620	342	272	352	272	D	273	D	1.00
36	MAS3	DF-W	3.20	2.00	0.63	300	30	1	384	SFRM4	276	1467	47	1139	586	537	686	537	D	470	D	1.14
37	MAS3	DF-W	5.00	2.00	0.40	300	30	1	525	SFRM4	379	2967	47	1779	1268	913	1286	913	D	812	D	1.12
38	MAS4	DF-W	2.01	2.23	1.11	200	60	1	418	SFRM1	229	529	51	1340	521	415	500	415	D	454	D	0.91
39	MAS4	DF-W	2.01	2.23	1.11	200	30	2	418	SFRM1	229	529	51	1340	521	415	500	415	D	502	D	0.83
40	MAS4	DF-W	3.01	2.23	0.74	200	60	1	626	SFRM1	343	1175	51	2007	1168	699	990	699	D	853	D	0.82
41	MAS4	DF-W	4.01	2.23	0.56	200	60	1	834	SFRM1	457	1963	51	2674	2074	1010	1569	1010	D	1289	D	0.78
42	MAS4	DF-W	5.01	2.23	0.45	200	60	1	1042	SFRM1	570	2847	51	3341	3237	1322	2208	1322	D	1998	D	0.66
43	MAS4	DF-W	1.01	2.23	2.21	200	60	1	210	SFRM1	115	96	66	673	132	239	145	132	F	160	F	0.82
44	MAS4	DF-W	2.01	2.23	1.11	200	60	1	418	SFRM5	180	491	51	1340	408	375	476	375	D	435	D	0.86
45	MAS4	DF-W	2.01	2.23	1.11	200	30	2	105	SFRM5	64	340	48	1340	153	324	256	153	F	236	F	0.65
46	MAS4	DF-W	3.01	2.23	0.74	200	30	2	157	SFRM5	96	750	47	2007	342	562	535	343	F	469	F	0.73
47	MAS4	DF-W	4.01	2.23	0.56	200	30	2	209	SFRM5	128	1274	47	2674	607	824	886	608	F	668	D	0.91
48	MAS4	DF-W	5.01	2.23	0.45	200	30	2	261	SFRM5	160	1890	47	3341	948	1086	1294	949	F	927	D	1.02
49	MAS4	DF-W	1.01	2.23	2.21	200	30	2	53	SFRM5	32	77	66	673	39	184	70	39	F	67	F	0.57
50	MAS4	DF-W	7.01	2.23	0.32	200	30	2	365	SFRM5	224	3325	47	4674	1855	1611	2239	1611	D	1375	D	1.17
51	MAS4	DF-W	2.01	2.23	1.11	200	20	1	105	SFRM6	81	575	48	673	95	215	153	95	F	142	F	0.67

(*continued on next page*)

Table 4 (*continued*)

Ref. #	URM ID	Wall restr.[1]	L [m]	h [m]	h/L [-]	t_m [mm]	t_{coat} [mm]	n [-]	N [kN]	SFRM ID	Proposed analytical model								Numerical		$\frac{V_R^{an}}{V_R^{num}}$
											x_f [mm]	x_s [mm]	θ [°]	$V_{R,max}$ [kN]	$V_{R,flex}$[2] [kN]	$V_{R,t}$ [kN]	$V_{R,s}$ [kN]	V_R^{an} [kN]	Fail. mode[3]	V_R^{num} [kN]	Fail. mode[3]	
52	MAS4	DF-W	2.01	2.23	1.11	200	20	1	418	SFRM6	315	860	49	673	334	280	334	280	D	272	D	1.03
53	MAS4	DF-W	3.01	2.23	0.74	200	20	1	157	SFRM6	121	1234	46	1008	213	373	302	213	F	281	F	0.76
54	MAS4	DF-W	3.01	2.23	0.74	200	20	1	626	SFRM6	471	1835	49	1008	748	470	606	470	D	518	F	0.91
55	MAS4	DF-W	4.01	2.23	0.56	200	20	1	209	SFRM6	161	2024	46	1343	378	535	476	378	F	408	D	0.93
56	MAS4	DF-W	4.01	2.23	0.56	200	20	1	834	SFRM6	628	2930	49	1343	1327	660	902	660	D	916	D	0.72
57	MAS4	DF-W	5.01	2.23	0.45	200	20	1	261	SFRM6	202	2901	46	1677	590	697	667	591	F	542	D	1.09
58	MAS5	C-W	3.00	1.97	0.66	200	20	2	250	SFRM1	293	560	48	1140	327	446	337	327	F	297	F	1.10
59	MAS5	C-W	3.00	1.97	0.66	200	20	1	250	SFRM1	365	634	48	708	246	287	247	246	F	219	F	1.12
60	MAS5	C-W	3.00	1.97	0.66	200	20	2	500	SFRM1	450	679	50	1140	479	470	488	470	D	402	F-D	1.17
61	MAS5	C-W	3.00	1.97	0.66	200	20	1	125	SFRM1	238	520	46	708	166	264	170	166	F	157	F	1.06
62	MAS5	C-W	3.00	1.97	0.66	200	20	1	62.5	SFRM1	174	456	46	708	124	249	131	124	F	94	F	1.32
63	MAS5	C-W	4.90	1.97	0.40	200	20	2	250	SFRM3	234	1219	47	1862	433	705	616	433	F	409	F	1.06
64	MAS5	C-W	4.90	1.97	0.40	200	20	1	250	SFRM3	320	1396	47	1156	360	439	424	360	F	294	F	1.23
65	MAS5	C-W	4.90	1.97	0.40	200	20	1	500	SFRM3	582	1823	48	1156	625	481	622	481	D	463	F-D	1.04
66	MAS5	C-W	3.00	1.97	0.66	240	25	2	270[4]	SFRM7	187	220	48	1081	195	453	196	195	F	214	F	0.91
67	MAS5	C-W	3.00	1.97	0.66	200	25	2	265[4]	SFRM7	290	221	48	1026	309	433	317	309	F	312	F	0.99
68	MAS5	DF-W	1.25	1.40	1.12	200	30	1	55[4]	SFRM1	121	250	48	385	136	117	148	117	D	126	D	0.93

[1] Wall restraints: C-W = cantilever wall; DF-W = double fixed-end wall.
[2] $V_{Rd,flex} = M_{Rd}/(\beta h)$ ($\beta = 0.5$ for double fixed-end walls; $\beta = 1$ for cantilever walls) is the lateral load causing flexural failure of the member.
[3] Failure mode notation: F = flexure; D = diagonal shear; S = sliding shear.
[4] The axial load includes the weight of the masonry panel strengthened with coating.

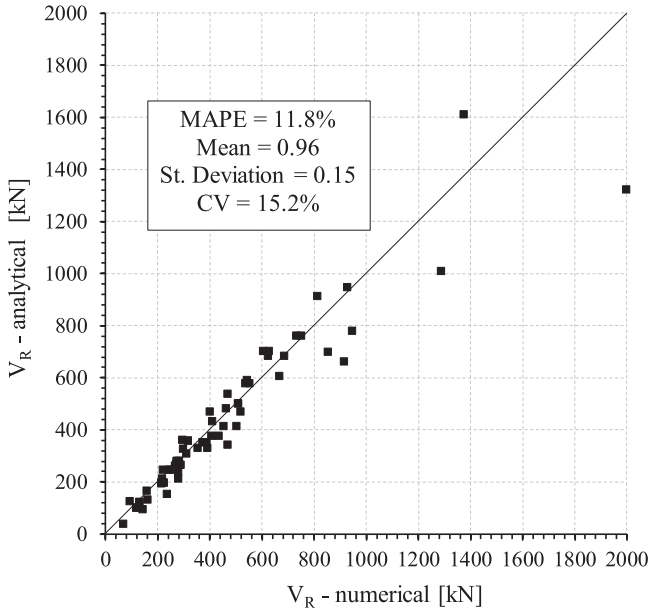

Fig. 10. Analytical vs numerical prediction of total lateral resistance (V_R).

Ø = 8 mm is the bar diameter;
c_{min} = 8.5 mm is the minimum cover;
c_{max} = 125 mm is the maximum cover.

When splitting failure occurs, the maximum tensile stress acting in each rebar can be estimated as follows:

$$\sigma_{s,max} = \min\left(4\cdot\tau_{bu,split}\cdot\frac{L_b}{Ø}\ ;\ f_y\ ;\ 2.5\cdot\sqrt{f_{cm}}\cdot4\cdot\frac{L_b}{Ø}\right) = 218\,\text{MPa} \quad (20)$$

where f_y = 620 MPa is the yield strength of the rebars used in the experimental test and L_b = 40 mm is the maximum bonded length assumed equal to 5Ø. Therefore, to take into account the effect of splitting cracks in the calculation of the flexural resistance of the wall #67, the maximum stress $\sigma_{s,max}$ was used in the Eqs. (17) and (18) to limit the maximum stress acting in the rebars.

The sliding shear resistance of the wall #67 was calculated by including the dowel resistance of all (i.e., 16 rebars) vertical rebars intersecting the base section of the members. As the cross-section area of a single rebar is 50.2 mm^2, the total area $\sum A_{sn}$ is equal to 803 mm^2.

Table 4 reports also the predicted resistance of the wall #68, which was one of the bearing walls forming the test building described in Section 3.1. Note that in addition to the properties summarized in Table 4, the wall was reinforced with one 8 mm diameter rebar located close to each toe of the base section, which laid at the same level of the bottom side of the two windows. These rebars had a yield strength of 620 MPa and were both inclined at 45° to the base section. To get an accurate description of the reinforcement layout one may refer to [18].

Considering the results of Table 4, one can observe that the analytical predictions of resistance and failure mode of the walls #66, #67 and #68, were all very close to those observed in the experimental tests described in Section 3.1. This result represents a further proof of the model reliability.

4. Worked example

A step-by-step application of the analytical model is carried out for the wall #66 tested in [36]. As detailed in Table 4, the specimen is a cantilever hollow block masonry (MAS5 - Table 1 and Table 3) wall having a length L = 3000 mm, an effective height h = 1970 mm and a thickness t_m = 240 mm. Each side of the wall (n = 2) is strengthened with a 25 mm thick (t_{coat}) layer of mortar SFRM7 (Table 2) not connected to the foundation. The axial load (N) acting at the base of the

member is 270 kN, corresponding to an axial stress of 0.38 MPa. The mechanical properties used in the calculation are summarized below. Note that the mean values obtained from characterization tests were used as the aim is to compare the analytical results with the experimental ones.

Masonry (MAS5):
- $f_m = 2.3$ MPa;
- $f_{mt} = 0.09$ MPa.
- $f_{v0} = 0.20$ MPa.

SFRM (SFRM7):
- $f_c = 25$ MPa;
- $f_{ct} = 1.65$ MPa;
- $f_{Ft\text{-}0.25} = 1.68$ MPa;
- $f_{Ftu} = 1.25$ MPa.

4.1. Shear resistance

According to Eq. (1), the shear resistance is the lowest of the resisting shear related to the diagonal tension ($V_{R,t}$) and sliding ($V_{R,s}$) mechanisms.

4.1.1. Diagonal shear resistance

The diagonal shear resistance is obtained from Eq. (2) as the combination of the resistances due to masonry and SFRM coating, provided that the maximum resistance $V_{R,max}$ is not exceeded. By taking $b = 1$ ($h/L = 0.66 < 1$) and $\sigma_0 = N/(L \cdot t_m) = 0.38$ MPa, the diagonal shear resistance of masonry is obtained from Eq. (5):

$$V_{t,m} = 3000 \cdot 240 \cdot \frac{0.09}{1} \cdot \sqrt{1 + \frac{0.38}{0.09}} = 147\,\text{kN} \tag{21}$$

According to Eq. (10), the shear stress corresponding to first cracking of coating is:

$$v_{cr} = \frac{1.65}{1} \cdot \sqrt{1 + \frac{0.38}{1.65}} = 1.83\,\text{MPa} \tag{22}$$

The average slope of the struts θ (Eq. (11)) results from the following calculation:

$$\theta = \min\left[\arctan\left(\frac{1.65 + 0.38}{1.83}\right) ; 90^\circ\right] = 48^\circ > 33^\circ = \arctan\left(\frac{1970}{3000}\right) \tag{23}$$

Considering the angle θ reported above, the design residual tensile strength (see Eq. (9)) $f_{Ft} = \max(0.9 \cdot 1.65; 1.68) = 1.68$ MPa of SFRM7 and the factor $m = \max[1; (2 \cdot 3000/1970 - 1)] = 2.05$, the diagonal shear resistance of coating results from the Eq. (6):

$$V_{t,coat} = 2.05 \cdot 1.68 \cdot 2 \cdot 25 \cdot \frac{1970}{2 \cdot \sin^2(48^\circ)} = 306\,\text{kN} \tag{24}$$

Given the compressive strength of MAS5 and SFRM7, the factor k is calculated from the Eq. (4):

$$k = \frac{240 + 2 \cdot 25 \cdot 25/2.3}{240 + 2 \cdot 25} = 2.7 \tag{25}$$

Consequently, the maximum shear resistance (see Eq. (3)) of the wall related to diagonal crushing of masonry is:

$$V_{R,max} = 0.25 \cdot 2.7 \cdot 2.3 \cdot (240 + 2 \cdot 25) \cdot 0.8 \cdot 3000 = 1081\,\text{kN} \tag{26}$$

Thus, according to Eq. (2), the total shear resistance of the strengthened panel is:

$$V_{R,t} = \min(147 + 306 ; 1081) = 453\,\text{kN} \tag{27}$$

4.1.2. Sliding shear resistance

To calculate the resistance due to the shear sliding mechanism, the frictional contributions of coating ($v_{s,coat}$) and masonry ($v_{s,m}$) must be determined. The first one (see Eq. (13)) is equal to:

$$v_{s,coat} = 0.5 \cdot 0.56 \cdot 25 = 7.0\,\text{MPa} \tag{28}$$

where $\eta = 0.6 \cdot (1 - (25 - 8)/250)) = 0.56$.

The latter depends on the length of the compressed zone (x_s), according to Eq. (14):

$$v_{s,m} = 0.4 \cdot 5.11 + 0.2 = 2.24 \tag{29}$$

where $\sigma_{0,s} = 270000/(240 \cdot x_s) = 5.11$ MPa and $f_{v0} = 0.2$ MPa. Assuming $\beta = 1$, suitable for the analyzed cantilever wall, the length x_s is calculated by Eq. (15), which reads as follows:

$$8.73 \cdot 10^5 \cdot x_s - 1.92 \cdot 10^8 = 0 \Rightarrow x_s = 220\,\text{mm} \tag{30}$$

As no connector between coating and the wall foundation is provided ($V_d = 0$), the parameters calculated above can be included in the Eq. (12) to get the total sliding shear resistance:

$$V_{R,s} = 220 \cdot (7.0 \cdot 2 \cdot 25 + 2.24 \cdot 240) = 196\,\text{kN} \tag{31}$$

In conclusion, the total lateral shear resistance of the wall is:

$$V_R = \min(453 ; 196) = 196\,\text{kN} \tag{32}$$

4.2. Flexural resistance

By rearranging the Eq. (17) and neglecting the terms related to the vertical reinforcement, the neutral axis depth (x_f) results:

$$x_f = 270000/(1 \cdot 0.8 \cdot (2.3 \cdot 240 + 25 \cdot 2 \cdot 25)) = 187\,\text{mm} \tag{33}$$

Note that the calculation of x_f does not consider the tensile contribution of coating (f_{Ftu}) as it was not connected to the foundation. Moreover, the coefficient α was assumed equal to 1 (as for all the walls of the parametric study) as the long term effects are neglected.

The design resisting moment (M_R) is obtained from Eq. (18):

$$M_R = -\frac{1 \cdot (2.3 \cdot 240 + 25 \cdot 2 \cdot 25) \cdot (0.8 \cdot 187)^2}{2} + \frac{270000 \cdot 3000}{2} = 385\,\text{kNm} \tag{34}$$

which corresponds to a total lateral load of:

$$V_{R,flex} = M_R/(\beta h) = 195\,\text{kN} \tag{35}$$

Being the lowest value among those calculated before, the flexural resistance corresponds to the total lateral resistance of the wall (V_R) reported in Table 4.

5. Concluding remarks

In this paper, code-oriented formulations for calculating the in-plane lateral resistance of walls strengthened by SFRM overlays were derived and mainly validated by comparison with the numerical results obtained from a comprehensive parametric study. The analytical model herein proposed is consistent with the MC2010 recommendations for fiber reinforced concrete materials.

Equations for determining the diagonal shear, the sliding shear and the flexural resistance of URM panels strengthened with SFRM overlay were proposed.

Based on the results of the validation procedure performed against comparison with the numerical simulations of 68 walls, three of which (i.e. wall #66, #67 and #68) were also investigated by experimental tests performed by the Authors, the following main conclusions can be drawn:

- The proposed model appeared able to provide reasonable estimations of both the in plane strength (MAPE = 11.7 %) and failure mode of the strengthened walls. The failure mode predicted by the analytical model was consistent with the numerical/experimental one for 58 of the 68 walls. The results of the tests further support the

suitability of the analytical predictions resulting from the proposed model.

- The inaccuracy of the model seems to increase especially when very squat walls ($h/L < 0.5$) are considered. However, irrespective of the wall aspect ratio, the analytical predictions are generally more conservative than the corresponding numerical ones.
- The worked example reported in the paper showed that the model can be easily implemented and does not require a significant calculation effort. Thus, it is suitable for the inclusion in structural guidelines used for practical design.

It is worth remarking that the experimental results available at the moment are still limited. To fill this gap, additional tests on repaired and strengthened walls will be performed to improve the experimental database and further check the validity of the proposed equations.

Declaration of Competing Interest

The authors declare that they have no known competing financial interests or personal relationships that could have appeared to influence the work reported in this paper.

Data availability

Data will be made available on request.

Acknowledgements

The present research work is part of the Health&Wealth project "Sismacomf" supported by the University of Brescia and by Tecnologia e Ricerca Italiana S.r.l. (TRI S.r.l). The financial support provided by the RELUIS-DPC project 2019–2021 is also gratefully acknowledged.

References

[1] Corradi M, Tedeschi C, Binda L, Borri A. Experimental evaluation of shear and compression strength of masonry wall before and after reinforcement: Deep repointing. Constr Build Mater 2008;22(4):463–72.
[2] Corradi M, Di Schino A, Borri A, Rufini R. A review of the use of stainless steel for masonry repair and reinforcement. Constr Build Mater 2018;181:335–46.
[3] Valluzzi MR, Tinazzi D, Modena C. Shear behavior of masonry panels strengthened by FRP laminates. Constr Build Mater 2002;16(7):409–16.
[4] Tomaževič M, Klemenc I, Weiss P. Seismic upgrading of old masonry buildings by seismic isolation and CFRP laminates: a shaking-table study of reduced scale models. Bull Earthq Eng 2009;7(1):293–321.
[5] Gattesco N, Boem I. Experimental and analytical study to evaluate the effectiveness of an in-plane reinforcement for masonry walls using GFRP meshes. Constr Build Mater 2015;88:94–104.
[6] Monaco Alessia, et al. Finite element analysis of the out-of-plane behavior of FRP strengthened masonry panels. Compos Part B: Eng 2017;115:188–202. https://doi.org/10.1016/j.compositesb.2016.10.016.
[7] Lin YW, Wotherspoon L, Scott A, Ingham JM. In-plane strengthening of clay brick unreinforced masonry wallettes using ECC shotcrete. Eng Struct 2014;66:57–65.
[8] Dehghani A, Nateghi-Alahi F, Fischer G. Engineered cementitious composites for strengthening masonry infilled reinforced concrete frames. Eng Struct 2015;105:197–208.
[9] Giaretton M, Dizhur D, Garbin E, Ingham JM, da Porto F. In-plane strengthening of clay brick and block masonry walls using textile-reinforced mortar. J Compos Constr 2018;22(5).
[10] Kouris LAS, Triantafillou TC. State-of-the-art on strengthening of masonry structures with textile reinforced mortar (TRM). Constr Build Mater 2018;188:1221–33.
[11] D'Ambrisi A, Feo L, Focacci F. Experimental and analytical investigation on bond between Carbon-FRCM materials and masonry. Compos B Eng 2013;46:15–20.
[12] Cascardi A, Micelli F, Aiello MA. FRCM-confined masonry columns: experimental investigation on the effect of the inorganic matrix properties. Constr Build Mater 2018;186:811–25.
[13] Facconi L, Minelli F, Lucchini S, Plizzari G. Experimental study of solid and hollow clay brick masonry walls retrofitted by steel fiber-reinforced mortar coating. J Earthquake Eng 2020;24(3):381–402.
[14] Sevil T, Baran M, Bilir T, Canbay E. Use of steel fiber reinforced mortar for seismic strengthening. Constr Build Mater 2011;25(2):892–9.
[15] Simoncello, N., Zampieri, P., Gonzalez-Libreros, J., & Pellegrino, C. (2019). Experimental behaviour of damaged masonry arches strengthened with steel fiber reinforced mortar (SFRM). Composites Part B: Engineering, 177.
[16] Del Zoppo M, Di Ludovico M, Balsamo A, Prota A. Experimental in-plane shear capacity of clay brick masonry panels strengthened with FRCM and FRM composites. J Compos Constr 2019;23(5):04019038.
[17] Lucchini SS, Facconi L, Minelli F, Plizzari G. Retrofitting unreinforced masonry by steel fiber reinforced mortar coating: uniaxial and diagonal compression tests. Mater Struct 2020;53(6):1–22.
[18] Lucchini SS, Facconi L, Minelli F, Plizzari G. Cyclic Test on a Full-Scale Unreinforced Masonry Building Repaired with Steel Fiber-Reinforced Mortar Coating. J Struct Eng 2021;147(6).
[19] Zampieri P, Simoncello N, Libreros JG, Pellegrino C. Bond behavior of steel fiber-reinforced mortar (SFRM) applied onto masonry substrate. Archives of Civil and Mechanical Engineering 2020;20(3):1–20.
[20] Najafgholipour MA, Dehghan SM, Kamrava AR. In-plane shear behavior of masonry walls strengthened with steel fiber-reinforced concrete overlay. Asian Journal of Civil Engineering 2018;19(5):553–70.
[21] Italian Building Code, D.M. 17/01/2018. Technical code for constructions. Italian Ministry of Infrastructures and Transportation: Rome, Italy, 2018 (in Italian).
[22] fib Bulletin 65, Model Code 2010, Final Complete Draft. International Federation for Structural Concrete (fib), 2012.
[23] EN 1996-1-1:2013, Eurocode 6: Design of masonry structures - Part 1-1: General rules for reinforced and unreinforced masonry structures. European Committee for Standardization, 2013.
[24] FEMA 273, NEHRP Guidelines for the Seismic Rehabilitation of Buildings. Basic procedures manual applied technology council (ATC). Washington DC, USA, 1997.
[25] Triantafillou TC, Antonopoulos CP. Design of concrete flexural members strengthened in shear with FRP. J Compos Constr 2000;4(4):198–205.
[26] Elgawady, M. (2004). Seismic in-plane behavior of URM walls upgraded with composites. Ph.D. thesis (No. 3111), EPFL, Lausanne, Switzerland.
[27] D'Ambra C, Lignola GP, Prota A. Simple method to evaluate FRCM strengthening effects on in-plane shear capacity of masonry walls. Constr Build Mater 2021;268:121125.
[28] Park R, Paulay T. Reinforced concrete structures. New York, N.Y.: John Wiley and Sons Inc; 1975.
[29] CNR DT 215, Istruzioni per la Progettazione, l'Esecuzione ed il Controllo di Interventi di Consolidamento Statico mediante l'utilizzo di Compositi Fibrorinforzati a Matrice Inorganica. Consiglio Nazionale delle Ricerche: Rome, Italy, 2020 (in Italian).
[30] Turnšek, V., & Čačovič, F. (1971). Some experimental results on the strength of brick masonry walls. In Proceedings of the 2nd international brick masonry conference (pp. 149-156). Stoke-on-Trent, British Ceramic Research Association.
[31] Italian Building Code Commentary, Circolare n.7 C.S.LL.PP. 21/01/2019. Commentary on Technical code for constructions. Italian Ministry of Infrastructures and Transportation: Rome, Italy, 2019 (in Italian).
[32] Walraven JC. Fundamental analysis of aggregate interlock. Journal of the Structural Division 1981;107(11):2245–70.
[33] Minelli F, Plizzari G. Derivation of a simplified stress–crack width law for Fiber Reinforced Concrete through a revised round panel test. Cem Concr Compos 2015;58:95–104.
[34] Amin A, Foster SJ, Gilbert RI, Kaufmann W. Material characterisation of macro synthetic fibre reinforced concrete. Cem Concr Compos 2017;84:124–33.
[35] EN 14651. (2007) Test Method for Metallic Fibre Concrete- Measuring the Flexural Tensile Strength (Limit of Proportionality (LOP), Residual). European Committee for Standardization: 17 pp.
[36] Lucchini SS. Steel fiber reinforced mortar for seismic retrofitting of unreinforced masonry buildings. Italy: University of Brescia, Brescia; 2019. Ph.D. Thesis.
[37] Lucchini, S., Facconi, L., Minelli, F., Plizzari, G. "Retrofitting a full-scale two-story hollow clay block masonry building by Steel Fiber Reinforced Mortar coating". Proc. of the 3rd FRC International Workshop Fibre Reinforced Concrete: from Design to Structural Applications, Desenzano, Lake Garda, Italy - June 28-30, 2018. (Extended Abstract on pp. 114-115). ISBN: 978-88-89252-44-4.
[38] EN 1992-1-1:2015, Eurocode 2: Design of concrete structures - Part 1-1: General rules and rules for buildings. European Committee for Standardization, 2015.
[39] EN 1998-1:2013, Eurocode 8: Design of structures for earthquake resistance - Part 1: General rules, seismic actions and rules for buildings. European Committee for Standardization, 2013.
[40] EN 1998-3:2005, Eurocode 8: Design of structures for earthquake resistance - Part 3: Assessment and retrofitting of buildings. European Committee for Standardization, 2005.
[41] Diana 10.4 (2020). User's manual. Delft, The Netherlands: TNO DIANA BV.
[42] Feenstra PH. Computational Aspects of Biaxial Stress in Plain and Reinforced Concrete. The Netherlands: Technische Universiteit Delft, Delft; 1993. PhD Thesis.
[43] Hordijk DA. Local approach to fatigue of concrete. The Netherlands: Technische Universiteit Delft, Delft; 1991. PhD Thesis.
[44] Thorenfeldt, E., Tomaszewicz, A. & Jensen, J. J. (1987). Mechanical properties of high-strength concrete and applications in design. In Proceedings of the Symposium on Utilization of High-Strength Concrete, Tapir, Trondheim, Norway.
[45] Rots JG. Computational modeling of concrete fracture. Delft, The Netherlands: Technische Universiteit Delft; 1988. Ph.D. Thesis.
[46] Oliveira DV, Araújo AS, Lourengo PB, Magenes G, Penna A. Modelling of the in-plane behaviour of stone masonry panels. In: Structural Analysis of Historical Constructions: Anamnesis, Diagnosis, Therapy, Controls. CRC Press; 2016. p. 265–71.
[47] Javed M, Magenes G, Alam B, Khan AN, Ali Q, Syed AM. Experimental seismic performance evaluation of unreinforced brick masonry shear walls. Earthquake Spectra 2015;31(1):215–46.

[48] Penna A, Mandirola M, Rota M, Magenes G. Experimental assessment of the in-plane lateral capacity of autoclaved aerated concrete (AAC) masonry walls with flat-truss bed-joint reinforcement. Constr Build Mater 2015;82:155–66.
[49] Petry S, Beyer K. Influence of boundary conditions and size effect on the drift capacity of URM walls. Eng Struct 2014;65:76–88.
[50] Crisci G, Ceroni F, Lignola GP. Comparison between Design Formulations and Numerical Results for In-Plane FRCM-Strengthened Masonry Walls. Applied Sciences 2020;10(14):4998.